

Novel 2-Aminobenzothiazole Derivatives: Docking, Synthesis, and Biological Evaluation as Anticancer Agents

Omar M. Salih, Mahmoud A. Al-Sha'er,* and Haneen A. Basheer

Cite This: *ACS Omega* 2024, 9, 13928–13950

Read Online

ACCESS |



Metrics & More

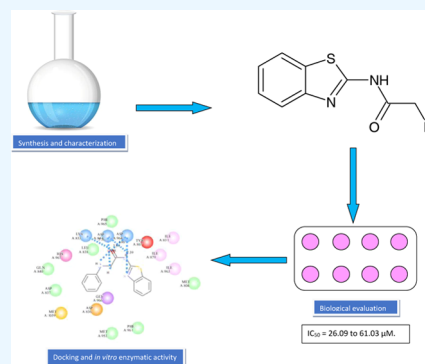


Article Recommendations



Supporting Information

ABSTRACT: Sixteen novel 2-aminobenzothiazole compounds with different amines or substituted piperazine moieties were designed, synthesized, and tested using various methods. Potential interactions were assessed by docking new compounds in the adenosine triphosphate (ATP) binding domain of the PI3K γ enzyme (PDB code: 7JWE) by nucleophilic substitution or solvent-free/neat fusion for docked compound synthesis. Final 2-aminobenzothiazole compounds were characterized by direct probe gas chromatography-mass spectrometry (GC-MS), proton ($^1\text{H-NMR}$), carbon-13 ($^{13}\text{C-NMR}$), and attenuated total reflectance-infrared Fourier transform infrared (ATR FT-IR). The synthesized compounds were investigated for anticancer activities on lung cancer (A549) and breast cancer (MCF-7) cell lines. The compounds' PI3K γ inhibition was evaluated at a 100 μM concentration. 4-Nitroaniline and piperazine-4-nitroaniline combination in OMS5 and OMS14 reduced lung and breast cancer cell line growth. IC_{50} values for OMS5 and OMS14, the strongest compounds, ranged from 22.13 to 61.03 μM . OMS1 and OMS2 inhibited PI3K γ at the highest rates (47 and 48%, respectively) at a 100 μM concentration. Results show that the PI3K γ enzyme suppression is not the main mechanism behind these OMS5 and OMS14 anticancer effects. CDK2, Akt, mTOR, and p42/44 MAPK are affected. EGF receptor suppression matters. AKT1, AKT3, CDK1/cyclin B, PDK1 direct, PIK3CA E542 K/PIK3R1 (p110 α /p85 α), PIK3CD/PIK3R1 (p110 δ /p85 α), and PKN inhibition were measured to evaluate the possible mechanism of compound OMS14. PIK3CD/PIK3R1 (p110 δ /p85 α) is the most, with 65% inhibition, suggesting a possible mechanism of anticancer properties. Furthermore, the NCI 60-cell line inhibition demonstrates promising broad anticancer inhibition against numerous cancer cell lines of OMS5 and OMS14, which could be good lead compounds for future development.



1. INTRODUCTION

Cancer is the second leading cause of death and is anticipated to climb 70% in 20 years.¹ Breast and lung cancers are two cancer types of interest since men's lung cancer ranks second after prostate cancer, and women's lung cancer follows breast cancer.² Breast cancer is the most common cancer worldwide, making it a global health issue. In 2020, 2.26 million cases were reported, making it common. Breast cancer is the leading cause of cancer mortality in women.³

The identification of cancer therapeutic targets is crucial; many cancer drug trials seek novel chemicals.⁴ One target is the PI3K/AKT/mTOR signaling system, which is crucial to cancer formation; this system is a frequently disturbed signaling pathway in cancer, making it a promising therapeutic target.⁵ There are various commercially marketed targeted inhibitors for specialized uses: everolimus, sirolimus, temsirolimus, alpelisib, duvelisib, copanlisib, idelalisib, and umbralisib. These are mTOR or PI3K inhibitors, with the latter being a targeted inhibitor. Cancer phase III trials have examined AKT inhibitors such as capivasertib and ipatasertib.^{6–8} These targeted drugs have shown promise in preclinical and clinical trials. Their therapeutic use is hampered by medication resistance.⁹ As cancer rates increase, more effective targeted drugs are needed. Integrating chemotherapeutic therapies or selectively targeted

pharmacological drugs targeting the PI3K/AKT/mTOR signaling pathway has also been demonstrated to inhibit malignant tumor proliferation.¹⁰

In a complex cellular signaling network, phosphoinositol-3-kinases (PI3Ks) govern metabolism, development, proliferation, and survival. AKT and mTOR are also included in the network.¹¹ Many cancer hallmarks are present in this signaling network's oncogenic aberrations, including upstream over-activation and genomic alterations.¹² Initial clinical trials of PI3K pan-isoform and dual PI3K/mTOR inhibitors for these proteins were plagued by ineffectiveness and severe reactions.¹³ Research has mostly focused on the four isoforms of class I PI3K signaling proteins: α , β , δ , and γ .

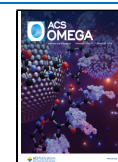
Research on mice with PI3K γ gene mutations indicates its significance in cell activation and migration in response to specific chemokines. PI3K γ signaling is significant in myeloid

Received: November 18, 2023

Revised: February 9, 2024

Accepted: February 28, 2024

Published: March 14, 2024



cells, downstream of GPCRs like chemokine receptors and RAS. Also, these cells can activate PI3K γ in response to tissue hypoxia. Research on PI3K γ deletion and kinase-dead knock-in mutants has shown its importance in the immune-suppressive tumor microenvironment, namely, in myeloid-derived cells. Myeloid cells in tumors may help them relapse after radiation or chemotherapy and spread to other regions of the body. Preclinical studies demonstrate the importance of PI3K γ in myeloid cell biology. Research suggests that inhibiting PI3K γ in tumor-associated myeloid cells may effectively prevent tumor growth in certain scenarios.¹⁴

Medicinal chemists search for molecules that can treat cancer on several targets.¹⁵ Benzothiazoles, which have benzene and thiazole rings, are utilized in numerous medicines worldwide. Chemical compounds like benzothiazoles and their heterocyclic derivatives have several biological impacts. Benzothiazole-derived drugs' wide range of medicinal qualities has inspired medicinal chemists to develop new therapeutic molecules. Anticancer, antibacterial, antidiabetic, anti-inflammatory, antiviral, antioxidant, antitubercular, antimalarial, antiasthmatic, anthelmintic, photosensitizing, diuretic, analgesic, and other properties have been reported in the benzothiazole ring system.¹⁶

2-Amino benzothiazoles are highly reactive for organic synthesis, including the construction of pharmacologically active heterocycles, due to the facile functionalization of the C2-NH₂ group and the benzene ring inside the benzothiazole ring.¹⁷

Many methods were developed to synthesize 2-aminobenzothiazole (Figure 1) and its derivatives. 2-Aminobenzothiazole

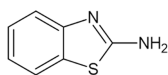


Figure 1. 2-Aminobenzothiazole scaffold.

thiazole is a key reactant or intermediary in the synthesis of fused heterocycles. The NH₂ and endocyclic N groups in 2-aminobenzothiazole are well-positioned to react with electrophilic reagents, forming a variety of fused heterocyclic compounds.¹⁸

Cancer is treated using chemotherapeutic drugs to limit its spread and tumor growth. The most serious side effects of chemotherapy for cancer treatment—gastrointestinal issues, infections, bleeding, and hair loss—are the biggest drawbacks. Therefore, medicinal chemists are interested in developing novel compounds that suppress cancer cells. A novel scaffold of 2-aminobenzothiazole derivatives will be introduced in this study to generate promising selective anticancer medicines. First, aminobenzothiazole is coupled with monochloroacetyl chloride at 0 °C using acetone to give (1-chloroacetyl)-2-aminobenzothiazole, which is then condensed with a particular amine to get the end product. Analgesic, anti-inflammatory, fungicidal, antimicrobial, anticancer, antileishmanial, anthelmintic, antirheumatic, central nervous system (CNS) antidepressant, and other activities are found in the benzothiazole scaffold.^{19–27} Many biological actions were observed in aminobenzothiazole derivatives. One derivative has *in vitro* anti-TB activity.²⁸ Others have *in vitro* antibacterial activity.²⁹

The researchers synthesized and screened a range of novel benzothiazole compounds to determine their antiproliferative properties.³⁰ Some of them showed antiproliferative activity by targeting many enzymes such as CDK2 enzyme,³⁰ AKT and

PI3K,³¹ mTOR and PI3K,³² EGFR,³³ caspases, Bcl-2, p42/44 MAPK, and AKT.³⁴

According to other research, piperazine derivatives (piperazinobenzopyranones) suppress the breast cancer resistance protein, which reduces anticancer drug efficacy.³⁵ Nucleoside analogs with a piperazine ring were tested for cytotoxicity on cancer cell lines. The compounds with the highest efficacy were next studied to determine their mechanism of action. By blocking kinase proteins, these medicines caused senescent cell death.³⁶ The benzothiazole–piperazine backbone's anticancer properties have shown that arylsulfonamides and arylthiol derivatives are cytotoxic to hepatocellular (HepG-2), prostate (DU-145), breast (MCF-7), and CD4 + human acute T-lymphoblastic leukemia (CCRF-CEM) cell lines.³⁷

Novel benzothiazole–piperazine compounds were tested for cytotoxicity using colon (HCT-116), breast (MCF-7), and liver cancer cell lines.³⁸ These studies show that many substituted benzothiazole–piperazine compounds are active against cancer cell types.³⁸ The objective of the study is to design new benzothiazole–piperazine compounds that have been successfully docked into the binding pocket of the PI3K enzyme; the highest-scored compounds are selected for further synthesis, purification, and instrumental validation, followed by *in vitro* enzyme assay and cell line inhibition MTT assay, in addition to submission of the best active compounds to the NCI 60-cell line screening program (Figures S1 and S2 in the Supporting Information).

2. MATERIALS AND METHODS

2.1. Materials. All reagents, catalysts, and chemicals utilized in the study were of analytical quality and supplied by commercial providers. The chemicals used in this study were sourced from various suppliers. 2-Aminobenzothiazole (Sigma-Aldrich, 99%), sulfapyridine (NENTECH, U.K., 99%), sulfaguanidine (Tokyo Chemical Industry, Japan, 98%), piperazine (Central Drug House, India, 99%), benzylamine (Loba Chemi, India, 99%), cyclohexylamine (Sigma-Aldrich, 99%), 3,4 dimethylaniline (GCC, U.K., 98%), 4-chloroaniline (Sigma-Aldrich, 98%), 4-bromoaniline (Sigma-Aldrich, 90%), 4-fluoroaniline (Sigma-Aldrich, 99%), 4-nitroaniline (Janssen, Belgium, 98%), diethylamine (GCC, U.K., 98%), *m*-toluidine (Sigma-Aldrich, 99%), morpholine (Tokyo Chemical Industry, Japan, 99%), dimethylformamide (DMF) (Carlo Erba, France, 99.9%), acetone (Carlo Erba, France, 99%), triethylamine (TEA) (TEDIA, 99%), ethanol (Carlo Erba, France, 98%), *n*-hexane (Carlo Erba, France, 95%), sodium bicarbonate (NaHCO₃) (GCC, U.K., 99.5%), sodium hydroxide (NaOH) (GCC, U.K., 99.5%), chloroform (Carlo Erba, France, 99.9%), and dimethyl sulfoxide (DMSO) (Carlo Erba, France, 99%) and monochloroacetyl chloride (α Chemika, India) were used.

2.2. Apparatus and Equipment. The study utilized various apparatus and equipment, including the Hei-Tec heating magnetic stirrer, manufactured by Heidolph in Germany, an HR-100A analysis scale (A & D), a vacuum pump MZ 2C NT model manufactured by Vacuubrand, a company based in Germany, a type Z 326 benchtop centrifuge (Hermle Labortechnik, Germany), a heating mantle, manufactured by Electrothermal Engineering in the United Kingdom, a 3608 vacuum oven (Thermo Fisher), a WFH-203B UV analyzer (China), an inverted microscope (OPTIKA, Italy), a CO₂ incubator, a Luna-FLTM Fluorescence Cell Counter L20001 (Korea), precasted TLC sheets (ALUGRAM, Germany), a GloMax Multi detection system (Promega), an AvanceCore

NMR spectrometer (Bruker, Germany), an Optronic Melting Point Meter M3000 (KRÜSS, Germany), a PerkinElmer spectrum two FT-IR spectrometer (PerkinElmer), and GC-MS (PerkinElmer).

2.3. Experimental Part. 2-Aminobenzothiazole was reacted with monochloroacetyl chloride in a round-bottom flask (1:1 equiv) with continuous stirring (RPM 300) under temperature (0–25 °C) and adding triethylamine (TEA) as a catalyst (overnight); on the second day, we get the final product by mixing the reaction mixture with ice, allowed to melt, and the mixture was filtrated to get the final product (P1) as a powder (Figure 2).

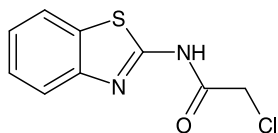


Figure 2. Compound P1.

According to Scheme 1, the chlorine atom of acetyl chloride was nucleophilically substituted with various amines and piperazine derivatives to create the final compounds (OMS1–OMS16) (Figures 3–18 and Table S1). A KRÜSS Optronic Melting Point Meter M3000 was used to measure the melting points of the synthesized compounds, including the intermediates. A PerkinElmer spectrum two FT-IR spectrometer (Diamond ATR FT-IR) (4000–400 $\text{cm}^{-1}/4 \text{ cm}^{-1}$ Spectral Resolution) was used to record the FT-IR spectra (USA) (Figures S3–S19). The final trisubstituted compounds' $^1\text{H-NMR}$ and $^{13}\text{C-NMR}$ spectra were captured at 300 and 75 MHz using a Bruker spectrometer (Al-Albays University-Jordan) (Figures S37–S70). The chemical shift in $^1\text{H-NMR}$ spectra was reported in ppm, and TMS was utilized as a reference. As a solvent, deuterated DMSO was employed. For $^1\text{H-NMR}$ and $^{13}\text{C-NMR}$, the run times were 2 min and 24 h, respectively. The evolution of the reactions was seen using precoated TLC sheets ALUGRAM Xtra SIL G/UV254 (Germany), with various ratios of (*n*-hexane: acetone) mixture as the mobile phase (see the Supporting Information). Liquid chromatography and tandem

Scheme 1. General Scheme of the Proposed Synthesis Reactions

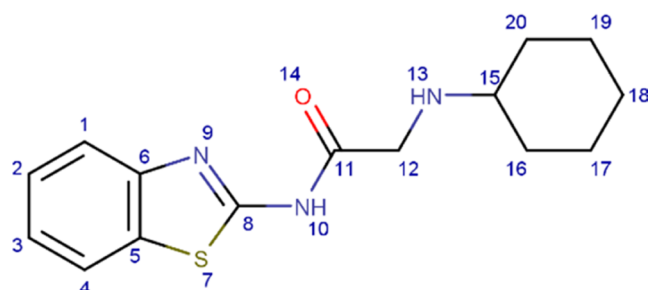
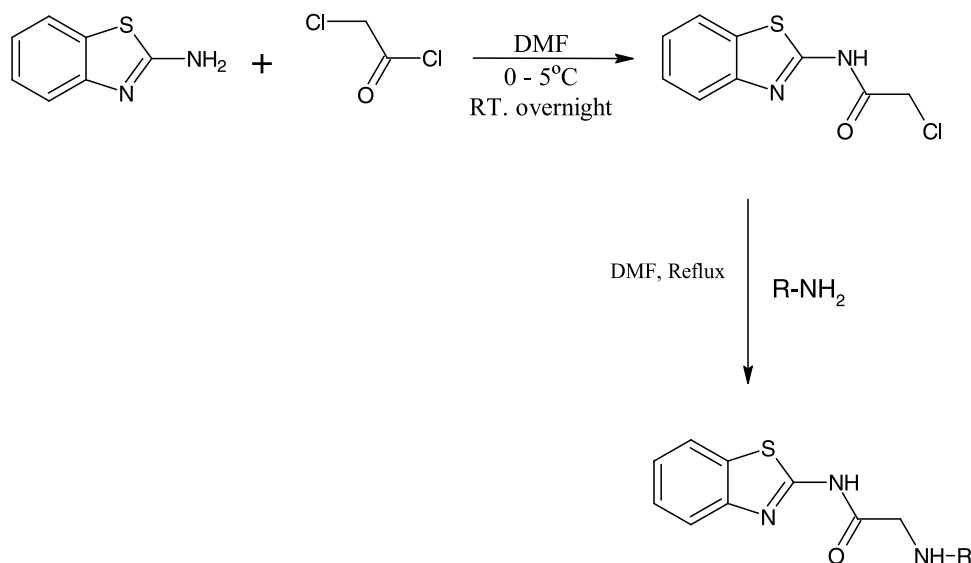


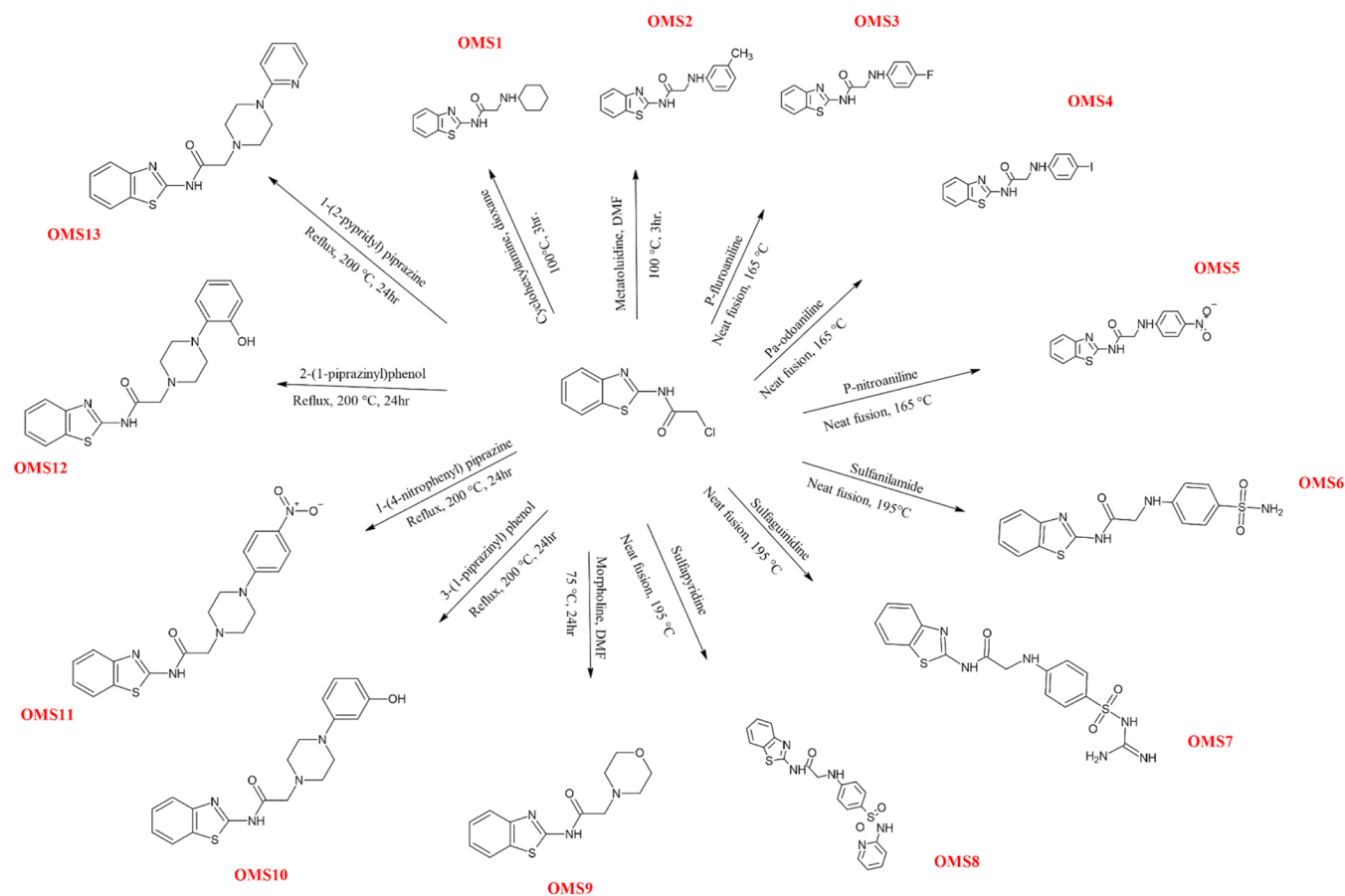
Figure 3. Chemical structure of OMS1.

mass spectrometry (LC-MS/MS) triple quad 8040 Shimadzu (Japan) were used to confirm the identity and purity of the compounds above 95% (Figures S20–S36).

2.3.1. Synthesis Procedure of Compounds OMS1–OMS13. According to Scheme 2, compounds OMS1–OMS13 were prepared by substitution of the chlorine atom in compound P1 with 13 different amines and piperazine derivatives (cyclohexylamine, meta-toluidine, 4-fluoroaniline, 4-iodoaniline, 4-nitroaniline, sulfanilamide, sulfaguanidine, sulfapyridine, morpholine, 1-(4-nitrophenyl) piperazine, 2-(1-piperazinyl) phenol, and 1-(2-pyridyl) piperazine).

2.3.1.1. Synthetic Procedure for Compound OMS1. To a magnetically stirred solution of compound P1 and cyclohexylamine (1:5 equiv) in 25 mL of dioxane, we increased the temperature to 100 °C and RPM 300. Following 3 h, the reaction mixture underwent a cooling process and subsequently underwent a washing procedure utilizing petroleum ether. After that, the crude product obtained after precipitation was separated using suction filtration and subsequently subjected to vacuum drying at a temperature of 30 °C for an extended period. The products *N*-(1,3-benzothiazol-2-yl)-2-(cyclohexylamino)acetamide was an off-white powder (yield 76.6%), M.P. 278–279 °C, FT-IR (ATR): 985, 1440, 1693, 2934, 3050, 3161 cm^{-1} , $^1\text{H-NMR}$ (300 MHz, DMSO) δ 10.54 (s, 1H, NH of N10), 4.15 (s, 1H, NH of N13), 3.46 (s, 2H, CH_2 of C12), 7.20–7.90 (m, 4H, CH of C1, C2, C3, & C4), 1.11–2.58 (m, 11H, CH_2 of C16, C17, C18, C19, C20 and CH of C15). $^{13}\text{C-NMR}$ (75 MHz, DMSO) δ 172.72 (C11), 159.93

Scheme 2. Synthetic Pathway of Compounds (OMS1–OMS13)



(C8), 148.8 (C6), 119.9–131.71 (C1, C2, C3, C4, and C5), 49.78 (C12), 55.82 (C15), 24.24–40.26 (C16, C17, C18, C19, and C20) ppm, GC-MS calculated 289.12 found MH^+ = 289.10 (Figures 3, S3, S20, S37, and S38).

2.3.1.2. Synthetic Procedure for Compound OMS2. To a magnetically stirred solution of compound P1 and metatoluidine (1:1 equiv) in 25 mL of DMF, we increased the temperature to 100 °C and RPM 300. After 24 h, the reaction mixture was carefully transferred onto a bed of ice and allowed to undergo the process of melting. Subsequently, the crude product obtained was separated using suction filtering and subjected to vacuum drying at a temperature of 30 °C for a duration of 1 night. The products *N*-(1,3-benzothiazol-2-yl)-2-(3-methylamino)acetamide was an off-white powder (yield 70.5%), M.P. 233–234 °C, FT-IR (ATR): 1467, 1651, 2947, 3091, 3327 cm^{-1} , 1H -NMR (300 MHz, DMSO) δ 10.193 (s, 1H, NH of N10), 7.19–8.03 (s, 1H, NH of N14) & (m, 8H, CH of C1, C2, C3, C4, C16, C17, C18, & C20), 5.40 (s, 2H, CH_2 of C12), 2.50 (s, 3H, CH_3 of C21). ^{13}C -NMR (75 MHz, DMSO) δ 168.72 (C11), 160.09 (C8), 145.24 (C15), 139.46 (C6), 39.44 (C12), 21.70 (C21), 114.35–127.28 (C1, C2, C3, C4, C5, C16, C17, C18, C19, & C20) ppm. GC-MS calculated 297.09 and found MH^+ = 297.08 (Figures 4, S4, S21, S39, and S40).

2.3.1.3. Synthetic Procedure for Compound OMS3. Compound OMS3 was prepared by neat fusion. One equivalent of P1 was subjected to a melting process within a crucible placed on a hot plate, with a temperature set at 165 °C. A total of five equivalents of *p*-fluoro-aniline were introduced into the molten substituted P1 compound, followed by stirring the resulting reaction mixture with a glass rod for 5–7 min at an identical

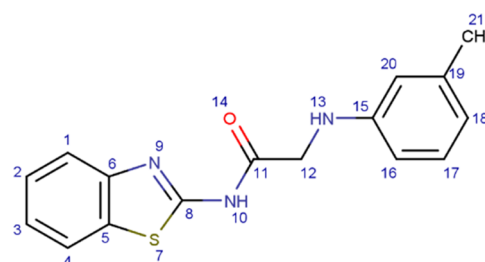


Figure 4. Chemical structure of OMS2.

temperature. Subsequently, the reaction mixture was permitted to cool to an ambient temperature. The mixture underwent many washes with acetone to eliminate any remaining excess of unreacted *p*-fluoro-aniline. The precipitated crude product was filtered and dried at room temperature. The products *N*-(1,3-benzothiazol-2-yl)-2-(4-fluoroanilino)acetamide was a dark green powder (yield 80%), M.P. 220–221 °C, FT-IR (ATR): 1008, 1650, 2941, 3057, 3301 cm^{-1} , 1H -NMR (300 MHz, DMSO) δ 10.00 (s, 1H, NH of N10), 7.22–7.91 (s, 1H, NH of N13) & (m, 8H, CH of C1, C2, C3, C4, C16, C17, C19, & C20), 3.81 (s, 2H, CH_2 of C12). ^{13}C -NMR (75 MHz, DMSO) δ 168.76 (C11), 160.11 (C8), 145.30 (C15), 39.43 (C12), 139.18 (C6), 114.27–127.31 (C1, C2, C3, C4, C5, C16, C17, C18, C19, & C20) ppm. GC-MS calculated 301.07 and found MH^+ = 301.01 (Figures 5, S5, S22, S41, and S42).

2.3.1.4. Synthetic Procedure for Compound OMS4. A neat fusion process synthesized compound OMS4. One equivalent of P1 was subjected to the process of melting within a crucible

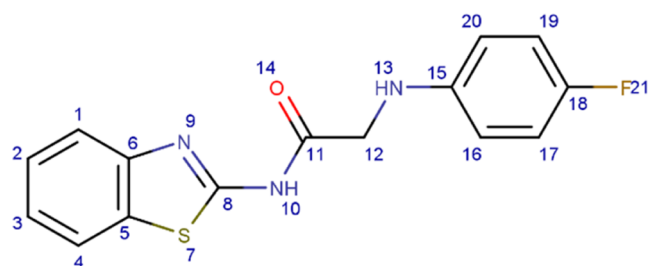


Figure 5. Chemical structure of OMS3.

placed on a heated plate operating at a temperature of 165 °C. Five equivalents of *p*-iodoaniline were introduced into the molten substituted P1, and the resulting mixture was agitated with a glass rod for 5–7 min at an identical temperature. Subsequently, the reaction mixture was permitted to reach an ambient temperature. The mixture underwent many washes with acetone to eliminate any remaining surplus of unreacted *p*-iodoaniline. The crude product obtained by precipitation was subjected to filtration and subsequently dried at an ambient temperature. The product *N*-(1,3-benzothiazol-2-yl)-2-(4-iodoanilino)acetamide was a light yellow powder (yield 80%), M.P. 200–201 °C, FT-IR (ATR): 1492, 1597, 2878, 3060 cm⁻¹, ¹H-NMR (300 MHz, DMSO) δ 11.21 (s, 1H, NH of N10), 6.87–8.29 (s, 1H, NH of N13) & (m, 8H, CH of C1, C2, C3, C4, C16, C17, C19, & C20), 3.81 (s, 2H, CH₂ of C12). ¹³C-NMR (75 MHz, DMSO) δ 168.62 (C11), 160.07 (C8), 145.47 (C15), 138.45 (C6), 39.44 (C12), 114.25–127.31 (C1, C2, C3, C4, C5, C16, C17, C18, C19, & C20) ppm. GC-MS calculated 408.97 and found MH⁺ = 409.00 (Figures 6, S6, S23, S43, and S44).

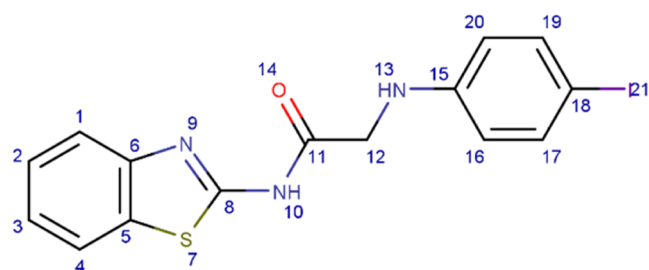


Figure 6. Chemical structure of OMS4.

2.3.1.5. Synthetic Procedure for Compound OMS5. A neat fusion process synthesized compound OMS5. A single equivalent of P1 was subjected to the process of melting within a crucible placed on a hot plate, with a temperature maintained at 165 °C. Five equivalents of 4-nitroaniline were introduced into the molten substituted P1, followed by stirring the reaction mixture with a glass rod at the identical temperature for 5–7 min. Subsequently, the reaction mixture was permitted to reach an ambient temperature. The entire mixture underwent many washes with acetone to eliminate any remaining unreacted 4-nitroaniline. The amino crude product obtained by precipitation was subjected to filtration and subsequently dried at an ambient temperature. The product *N*-(1,3-benzothiazol-2-yl)-2-(4-nitroanilino)acetamide was a yellow powder (yield 77.9%), M.P. 223–224 °C, FT-IR (ATR): 1314, 1508, 1598, 1712, 2923, 3075, 3365 cm⁻¹, ¹H-NMR (300 MHz, DMSO) δ 12.61 (s, 1H, NH of N10), 6.72–8.25 (s, 1H, NH of N13) & (m, 8H, CH of C1, C2, C3, C4, C16, C17, C19, & C20), 4.29 (s, 2H, CH₂ of

C12). ¹³C-NMR (75 MHz, DMSO) δ 168.77 (C11), 157.58 (C8), 154.25 (C15), 144.87 (C6), 39.76 (C12), 111.33–136.49 (C1, C2, C3, C4, C5, C16, C17, C18, C19, & C20) ppm. GC-MS calculated 328.06 and found MH⁺ = 328.04 (Figures 7, S7, S24, S45, and S46).

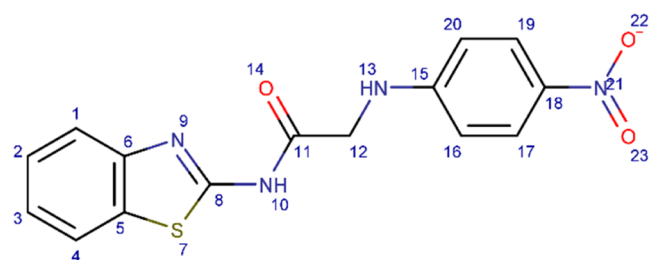


Figure 7. Chemical structure of OMS5.

2.3.1.6. Synthetic Procedure for Compound OMS6. A neat fusion process synthesized compound OMS6. A single equivalent of P1 was subjected to the process of melting within a crucible placed on a hot plate, with a temperature maintained at 195 °C. Five equivalents of sulfanilamide were introduced into the molten substituted P1, followed by stirring the reaction mixture with a glass rod at an identical temperature for 5–7 min. Subsequently, the reaction mixture was permitted to reach an ambient temperature. The entire mixture underwent many washes with acetone and diluted HCl to eliminate any remaining unreacted sulfanilamide. The crude product obtained by precipitation was subjected to filtration and subsequently dried at an ambient temperature. The product *N*-(1,3-benzothiazol-2-yl)-2-(4-sulfamoylanilino)acetamide was a white powder (yield 60.1%), M.P. 233–234 °C, FT-IR (ATR): 1151, 1302, 1694, 3072, 3239, 3339 cm⁻¹, ¹H-NMR (300 MHz, DMSO) δ 10.42 (s, 1H, NH of N10), 6.57–7.76 (s, 1H, NH of N14), (s, 2H, NH₂ of N22) & (m, 8H, CH of C1, C2, C3, C4, C16, C17, C19, & C20), 4.01 (s, 2H, CH₂ of C13). ¹³C-NMR (75 MHz, DMSO) δ 169.13 (C11), 151.05 (C8), 141.66 (C15), 138.39 (C6), 39.45 (C13), 111.17–130.89 (C1, C2, C3, C4, C5, C16, C17, C18, C19, & C20) ppm. GC-MS calculated 362.05 and found MH⁺ = 362.02 (Figures 8, S8, S25, S47, and S48).

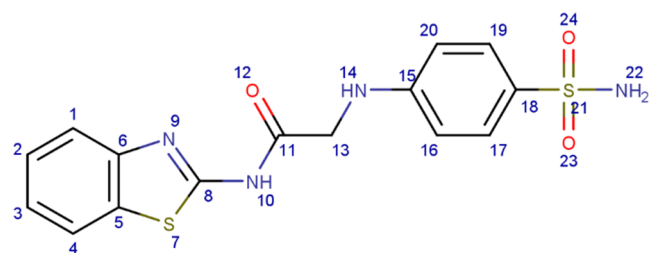


Figure 8. Chemical structure of OMS6.

2.3.1.7. Synthetic Procedure for Compound OMS7. A neat fusion process synthesized compound OMS7. Five equivalents of sulfaguanidine were subjected to the process of melting within a crucible placed on a hot plate, with a temperature maintained at 195 °C. One equivalent of P1 was introduced into the melted substituted sulfaguanidine, followed by stirring the reaction mixture with a glass rod at an identical temperature for 5–7 min. Subsequently, the reaction mixture was permitted to reach an ambient temperature. The entire mixture underwent many

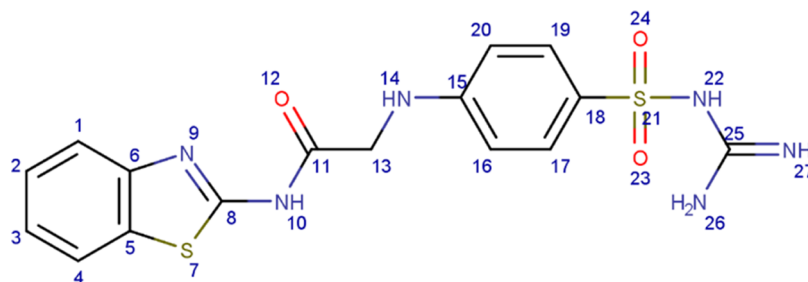


Figure 9. Chemical structure of OMS7.

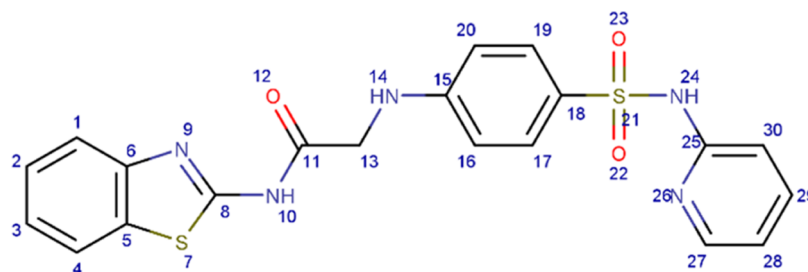


Figure 10. Chemical structure of OMS8.

washes with acetone and diluted HCl to eliminate any remaining unreacted sulfaguanidine. The crude product obtained by precipitation was subjected to filtration and subsequently dried at an ambient temperature. The product *N*-(1,3-benzothiazol-2-yl)-2-[4-(carbamimidoyl sulfamoyl)anilino]-acetamide was a red-brown powder (yield 31%), M.P. 235–236 °C, FT-IR (ATR): 1156, 1316, 1679, 2988, 3106, 3311 cm^{-1} , $^1\text{H-NMR}$ (300 MHz, DMSO) δ 11.04 (s, 1H, NH of N10), 6.58–7.99 (s, 1H, NH of N27), (s, 2H, NH_2 of N26) & (m, 8H, CH of C1, C2, C3, C4, C16, C17, C19, & C20), 4.01–5.33 (s, 2H, CH_2 of C13) & (s, 1H, NH of N14), 2.08 (s, 1H, NH of N22). $^{13}\text{C-NMR}$ (75 MHz, DMSO) δ 169.96 (C11), 157.81 (C8), 150.73 (C25), 149.31 (C15), 148.43 (C6), 39.72 (C13), 111.10–131.37 (C1, C2, C3, C4, C5, C16, C17, C18, C19, & C20) ppm. GC-MS calculated 404.07 and found MH^+ = 404.03 (Figures 9, S9, S26, S49, and S50).

2.3.1.8. Synthetic Procedure for Compound OMS8. A neat fusion process synthesized compound OMS8. Five equivalents of sulfapyridine were subjected to the process of melting within a crucible placed on a hot plate, with a temperature maintained at 195 °C. One equivalent of P1 was introduced into the molten substituted sulfapyridine, followed by stirring the reaction mixture with a glass rod at an identical temperature for 5–7 min. Subsequently, the reaction mixture was permitted to reach an ambient temperature. The entire mixture underwent many washes with acetone and diluted HCl to eliminate any remaining unreacted sulfapyridine. The crude product obtained by precipitation was subjected to filtration and subsequently dried at an ambient temperature. The product *N*-(1,3-benzothiazol-2-yl)-2-{4-[(pyridine-2-yl)sulfamoyl]anilino}-acetamide was a white powder (yield 41.4%), M.P. 210–211 °C, FT-IR (ATR): 1152, 1346, 1518, 1703, 3057, 3352 cm^{-1} , $^1\text{H-NMR}$ (300 MHz, DMSO) δ 11.11 (s, 1H, NH of N10), 10.7 (s, 1H, NH of N24), 6.63–8.09 (s, 1H, NH of N14) & (m, 12H, CH of C1, C2, C3, C4, C16, C17, C19, C20, C27, C28, C29 & C30), 4.17 (s, 2H, CH_2 of C13). $^{13}\text{C-NMR}$ (75 MHz, DMSO) δ 169.73 (C11), 157.60 (C8), 152.15 (C25), 151.59 (C27), 148.42 (C15), 145.76 (C6), 39.43 (C13), 111.17–139.19 (C1, C2, C3, C4, C5, C16, C17, C18, C19, C20, C28, C29, & C30)

ppm. GC-MS calculated 439.08 and found MH^+ = 439.07 (Figures 10, S10, S27, S51, and S52).

2.3.1.9. Synthetic Procedure for Compound OMS9. To a magnetically stirred solution of compound P1 and morpholine (1:5 equiv) in 25 mL of DMF, the temperature was increased to 75 °C and rotated to 300 rpm. Following 3 h, the reaction mixture was subsequently dumped onto ice, allowing for its dissolution. The resulting mixture was then subjected to a thorough washing process utilizing ether, followed by recrystallization employing the acetone/ether antisolvent method. The product *N*-(1,3-benzothiazol-2-yl)-2-(morpholin-4-yl)acetamide was white crystals (yield 55%), M.P. 148–149 °C, FT-IR (ATR): 1240, 1443, 1706, 2961, 3064, 3214 cm^{-1} , $^1\text{H-NMR}$ (300 MHz, DMSO) δ 12.02 (s, 1H, NH of N10), 2.28–3.72 (s, 2H, CH_2 of C13) & (m, 8H, CH_2 of C15, C16, C18 & C19), 7.29–8.00 (m, 4H, piperazine C2, C3 & C4). $^{13}\text{C-NMR}$ (75 MHz, DMSO) δ 169.28 (C11), 157.41 (C8), 148.41 (C6), 120.50–131.40 (C1, C2, C3, C4, & C5), 38.63–66.09 (C13, C15, C16, C18, & C19) ppm. GC-MS calculated 277.09 and found MH^+ = 277.02 (Figures 11, S11, S28, S53, and S54).

2.3.1.10. Synthetic Procedure for Compound OMS10. Compound P1 and 3-(1-piperazinyl) phenol were combined in a magnetically stirred solution with a 1:1 equiv ratio in 15 mL of *N,N*-dimethylformamide (DMF). Triethylamine (TEA) was then added as a catalyst in a 1:1 equiv ratio. The reaction mixture

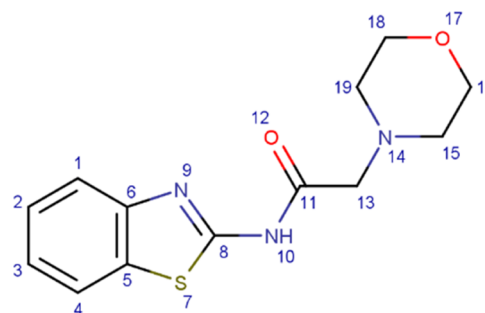


Figure 11. Chemical structure of OMS9.

was subjected to stirring for 10 min under ambient conditions. Following this, the reaction underwent reflux at a temperature of 200 °C for 4 h. Following the completion of the reaction, the reaction mixture was permitted to gradually reach an ambient temperature and subsequently transferred onto a mixture consisting of 75 mL of water and ice. The resulting precipitate was separated using the process of suction filtering, followed by drying under vacuum conditions at a temperature of 40 °C for a duration of 1 night. The product *N*-(1,3-benzothiazol-2-yl)-2-[4-(3-hydroxyphenyl)piperazin-1-yl]acetamide was an off-white powder (yield 64.8%), M.P. 255–256 °C, FT-IR (ATR): 1445, 1702, 3059, 3097, 3404 cm⁻¹, ¹H-NMR (300 MHz, DMSO) δ 12.33 (s, 1H, NH of N10), 9.15 (s, 1H, OH of O26), 2.68–3.42 (s, 2H, CH₂ of C13) & (m, 8H, CH₂ of C15, C16, C17, & C18), 6.23–8.00 (m, 8H, CH of C1, C2, C3, C4, C21, C22, C23, & C25). ¹³C-NMR (75 MHz, DMSO) δ 169.30 (C11), 158.04 (C8), 157.44 (C24), 152.32 (C20), 148.41 (C6), 102.45–131.41 (C1, C2, C3, C4, C5, C21, C22, C23, & C25), 38.62–60.12 (C13, C15, C16, C17, & C18) ppm. GC-MS calculated 368.13 and found MH⁺ = 368.19 (Figures 12, S12, S29, S55, and S56).

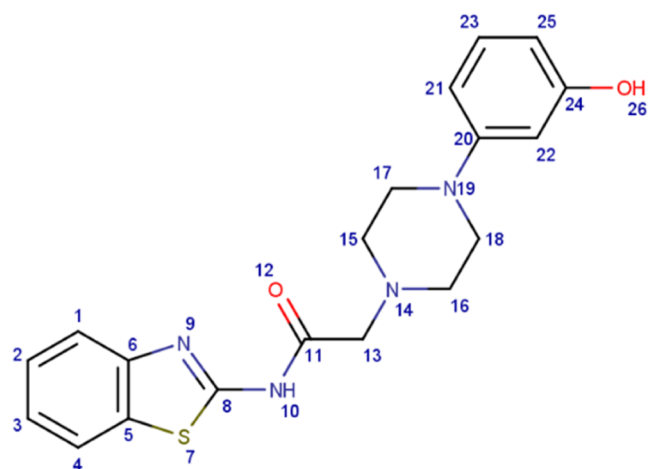


Figure 12. Chemical structure of OMS10.

2.3.1.11. Synthetic Procedure for Compound OM11. Compound P1 and 1-(4-nitrophenyl) piperazine were combined in a magnetically stirred solution with a 1:1 equiv ratio in 15 mL of *N,N*-dimethylformamide (DMF). Triethylamine (TEA) was then added as a catalyst in a 1:1 equiv ratio. The reaction mixture was subjected to stirring for 10 min under ambient conditions. Following this, the reaction underwent reflux at a temperature of 200 °C for 4 h. Following the completion of the reaction, the reaction mixture was permitted to gradually reach an ambient temperature and subsequently transferred onto a mixture consisting of 75 mL of water and ice. The resulting precipitate was separated using the process of suction filtering, followed by drying under vacuum conditions at a temperature of 40 °C for a duration of 1 night. The product *N*-(1,3-benzothiazol-2-yl)-2-[4-(4-nitrophenyl)piperazin-1-yl]acetamide was a yellow powder (yield 88%), M.P. 207–208 °C, FT-IR (ATR): 1334, 1598, 1708, 2966, 3063, 3225 cm⁻¹, ¹H-NMR (300 MHz, DMSO) δ 12.27 (s, 1H, NH of N10), 2.69–3.52 (m, 8H, CH₂ of C15, C16, C17, & C18), 7.03–8.08 (m, 8H, CH of C1, C2, C3, C4, C21, C22, C23, & C24), 4.47 (s, 2H, CH₂). ¹³C-NMR (75 MHz, DMSO) δ 169.35 (C11), 158.94 (C8), 157.44 (C25), 148.41 (C20), 147.55 (C6), 107.07–

137.51 (C1, C2, C3, C4, C5, C21, C22, C23, & C24), 38.63–60.48 (C13, C15, C16, C17, & C18) ppm. GC-MS calculated 397.12 and found MH⁺ = 397.15 (Figures 13, S13, S30, S57, and S58).

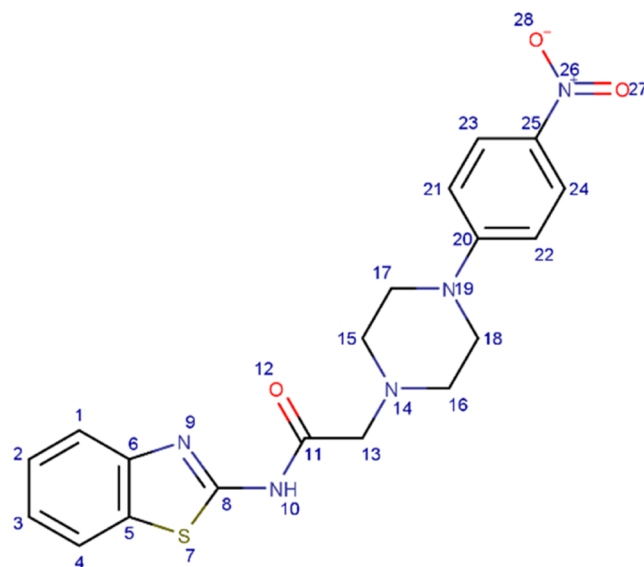


Figure 13. Chemical structure of OMS11.

2.3.1.12. Synthetic Procedure for Compound OM12. Compound P1 and 2-(1-piperazinyl) phenol were combined in a magnetically stirred solution with a 1:1 equiv ratio in 15 mL of *N,N*-dimethylformamide (DMF). Triethylamine (TEA) was then added as a catalyst in a 1:1 equiv ratio. The reaction mixture was subjected to stirring for 10 min under ambient conditions. Following this, the reaction underwent reflux at a temperature of 200 °C for 4 h. Following the completion of the reaction, the reaction mixture was permitted to gradually reach an ambient temperature and subsequently transferred onto a mixture consisting of 75 mL of water and ice. The resulting precipitate was separated using the process of suction filtering, followed by drying under vacuum conditions at a temperature of 40 °C for a duration of 1 night. The product *N*-(1,3-benzothiazol-2-yl)-2-[4-(2-hydroxyphenyl)piperazin-1-yl]acetamide was a red-brown powder (yield 90%), M.P. 260–261 °C, FT-IR (ATR): 1443, 1690, 2955, 3060, 3313 cm⁻¹, ¹H-NMR (300 MHz, DMSO) δ 11.10 (s, 1H, NH of N10), 9.33 (s, 1H, OH of O26), 4.48 (s, 2H, CH₂ of C13), 6.79–8.05 (m, 8H, CH of C1, C2, C3, C4, C21, C23, C24, & C25), 2.09–3.36 (m, 8H, CH₂ of C15, C16, C17, & C18). ¹³C-NMR (75 MHz, DMSO) δ 168.35 (C11), and 158.24 (C8), 150.12 (C22), 150.00 (C20), 138.52 (C6), 115.78–126.41 (C1, C2, C3, C4, C5, C21, C23, C24, & C25), 38.53–52.43 (C13, C15, C16, C17, & C18) ppm. GC-MS calculated 368.13 and found MH⁺ = 368.12 (Figures 14, S14, S31, S59, and S60).

2.3.1.13. Synthetic Procedure for Compound OM13. Compound P1 and 1-(2-pyridyl) piperazine were combined in a magnetically stirred solution with a 1:1 equiv ratio in 15 mL of *N,N*-dimethylformamide (DMF). Triethylamine (TEA) was then added as a catalyst in a 1:1 equiv ratio. The reaction mixture was subjected to stirring for 10 min under ambient conditions. Following this, the reaction underwent reflux at a temperature of 200 °C for 4 h. Following the completion of the reaction, the reaction mixture was permitted to gradually reach an ambient temperature and subsequently transferred onto a mixture

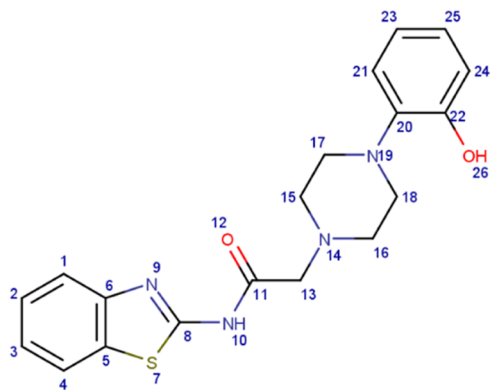


Figure 14. Chemical structure of OMS12.

consisting of 75 mL of water and ice. The resulting precipitate was separated using the process of suction filtering, followed by drying under vacuum conditions at a temperature of 40 °C for a duration of 1 night. The product *N*-(1,3-benzothiazol-2-yl)-2-[4-(pyridin-2-yl)piperazin-1-yl]acetamide was a rose gold powder (yield 87.4%), M.P. 184–185 °C, FT-IR (ATR): 1525, 1705, 2825, 2999, 3049, 3243 cm^{-1} , $^1\text{H-NMR}$ (300 MHz, DMSO) δ 12.18 (s, 1H, NH N10), 3.53 (s, 2H, CH_2), 6.62–8.12 (m, 8H, CH of C1, C2, C3, C4, C21, C23, C24, & C25), 2.64–3.53 (m, 8H, CH_2 of C15, C16, C17, & C18). $^{13}\text{C-NMR}$ (75 MHz, DMSO) δ 169.36 (C11), 158.94 (C8), 157.44 (C20), 148.41 (C24), 147.52 (C6), 107.07–137.50 (C1, C2, C3, C4, C5, C21, C23, & C25), 38.62–60.18 (C13, C15, C16, C17, & C18) ppm. GC-MS calculated 353.13 and found $\text{MH}^+ = 353.10$ (Figures 15, S15, S32, S61, and S62).

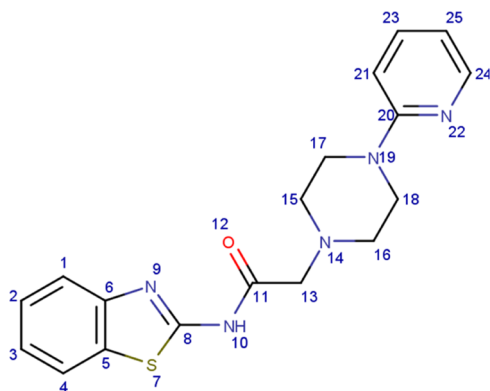


Figure 15. Chemical structure of OMS13.

2.3.2. Synthesis Procedure of Compounds OMS14–OMS16. Compound P2 was synthesized by substitution of the chlorine atom in P1 with piperazine (1:1 equiv ratio) in a 40 mL combination including equal quantities of acetone and water (RPM 250, temp. 60 °C overnight). After 24 h, the resulting

precipitate was separated from the reaction mixture using suction filtering and afterward subjected to vacuum drying at a temperature of 40 °C for a duration of 1 night (Scheme 3).

Intermediate P3 was prepared by adding monochloroacetyl chloride (1 equiv) to a 25 mL solution of 4-nitroaniline in DMF in an ice-bathed round-bottom flask and stirred overnight. The mixture was then poured into 100 mL iced water and filtrated to get the final product (Scheme 4).

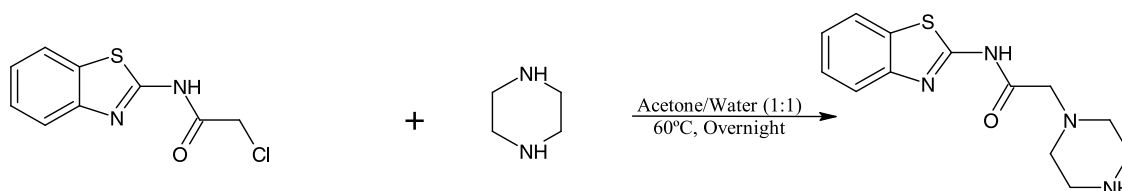
Triethylamine (TEA) was introduced into a solution of compound P2 and monochloroacetyl chloride (1 equiv) in 25 mL of dimethylformamide (DMF), which was magnetically agitated and kept in an ice bath. The addition of TEA occurred at a temperature of 0 °C. The experiment was conducted at a temperature of 0 °C and afterward allowed to progress at an ambient room temperature. Following 24 h, the reaction mixture was subjected to cooling and subsequently transferred onto a 100 mL mixture of ice and water. Intermediate P4 was obtained by performing suction filtering to separate the precipitated product, followed by vacuum drying at a temperature of 40 °C for an overnight period (Scheme 5).

The synthesis of compounds OMS14, OMS15, and OMS16 was prepared by extra steps mentioned separately in Schemes 6–8.

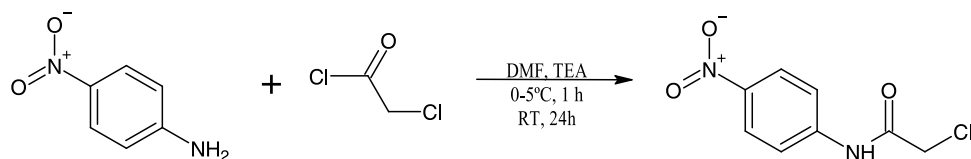
2.3.2.1. Synthetic Procedure for Compound OM14. Triethylamine (TEA) was added to a solution of compounds P2 and P3 (1 equiv) in 25 mL of DMF, which was magnetically agitated and placed in an ice bath. The addition of TEA occurred at a temperature range of 0–5 °C. The experiment was conducted at a temperature of 0 °C and thereafter allowed to progress at an ambient temperature. Following 24 h, the reaction mixture was subjected to a cooling process and subsequently transferred onto a 100 mL mixture of ice and water. The resulting product was separated using suction filtering and afterward subjected to vacuum drying at a temperature of 40 °C for a duration of 1 night. The product *N*-(benzo[*d*]thiazol-2-yl)-2-(4-(2-((4-nitrophenyl)amino)-2-oxoethyl)piperazin-1-yl)-acetamide was a bright yellow powder (yield 65.7%), M.P. 310–311 °C, FT-IR (ATR): 1266, 1443, 1530, 1694, 2992, 3278 cm^{-1} , $^1\text{H-NMR}$ (400 MHz, DMSO) δ 12.73 (s, 1H, NH of N10), 12.12 (s, 1H, NH of N22), 4.48 (s, 4H, CH_2 of C12 & C20), 2.64–2.89 (m, 8H, CH_2 of C15, C16, C17, & C18), 7.30–8.41 (m, 8H, CH of C3, C4, C5, C6, C25, C26, C27, & C28). $^{13}\text{C-NMR}$ (400 MHz, DMSO) δ 166.43 (C11), 158.06 (C21), 160.10 (C8), 148.87 (C1), 112.82–131.91 (C1, C2, C3, C4, C5, C24, C25, C26, C27, C28, & C29), 31.24 and 36.26 (C15, C16, C17, & C18), 43.3 (C20 & C12) ppm. GC-MS calculated 454.14 and found $\text{MH}^+ = 454.10$ (Figures 16, S16, S33, S63, and S64).

2.3.2.2. Synthetic Procedure for Compound OMS15. Compound P4 and piperazine (1 equiv) were combined in a 40 mL combination of acetone and water (equal parts) that was subjected to magnetic stirring and an ice bath. The reaction was carried out at a rotational speed of 250 rpm (RPM) and a

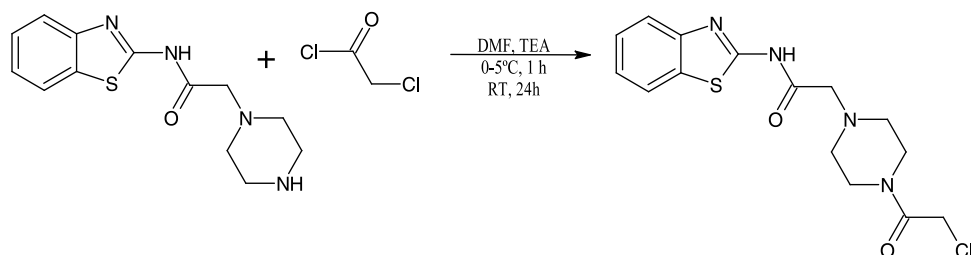
Scheme 3. Synthetic Pathway of Compound P2



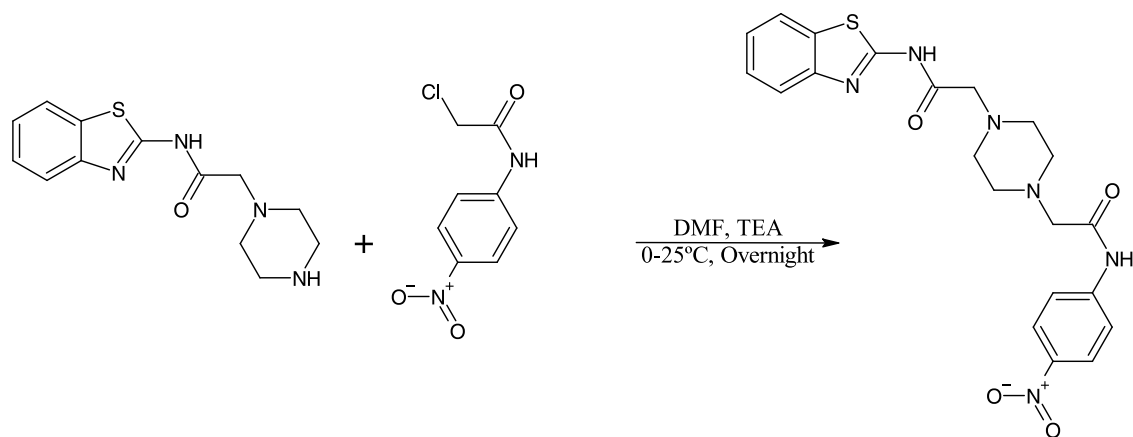
Scheme 4. Synthetic Pathway of Compound P3



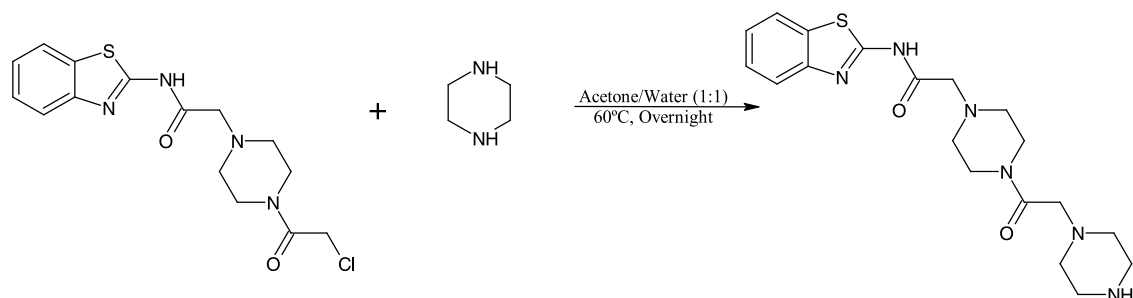
Scheme 5. Synthetic Pathway of Compound P4



Scheme 6. Synthetic Pathway of Compound OMS14



Scheme 7. Synthetic Pathway of Compound OMS15



temperature of 60 °C for an extended period, namely, overnight. Following 24 h, the precipitated product was separated by the utilization of suction filtering and subsequently subjected to vacuum drying at a temperature of 40 °C for the duration of the overnight period. The product *N*-(benzo[*d*]thiazol-2-yl)-2-(4-(2-oxo-2-(piperazin-1-yl)ethyl)piperazin-1-yl)acetamide was a white-yellow powder (yield 64.2%), M.P. 330–331 °C, FT-IR (ATR): 1463, 11697, 2987, 3046, 3353 cm⁻¹, ¹H-NMR (400 MHz, DMSO) δ 12.74 (s, 1H, N10), 4.48 (s, 4H, CH₂ of C12 & C21), 2.09–3.15 (m, 17H, CH₂ of C15, C16, C17, C18, C23, C24, C25, C26, & C27), 7.30–8.02 (m, 4H, CH of C3, C4, C5, & C6). ¹³C-NMR (400 MHz, DMSO) δ 166.41 (C11), 160.22 (C20), 158.05 (C8), 148.87 (C1), 121.17–131.19 (C2, C3, C4, C5, & C6), 43.03–65.11 (C12, C21, C15, C16, C17, C18, C23,

C24, C25, & C26) ppm. GC-MS calculated 402.18 and found MH⁺ = 402.20 (Figures 17, S17, S34, S65, and S66).

2.3.2.3. Synthetic Procedure for Compound OMS16. Triethylamine (TEA) was added to a solution of compounds P2 and P1 (1 equiv) in 25 mL of DMF, which was magnetically agitated and maintained in an ice bath at 0 °C. The experiment was conducted at a temperature of 0 °C and thereafter allowed to progress at an ambient temperature. Following 24 h, the reaction mixture was subjected to a cooling process and subsequently transferred onto a 100 mL mixture of ice and water. The resulting precipitate was separated from the reaction mixture using suction filtering and afterward subjected to vacuum drying at a temperature of 40 °C for a duration of 1 night. The product 2,2'-(piperazine-1,4-diyl)bis(*N*-(benzo[*d*]-

Scheme 8. Synthetic Pathway of Compound OMS16

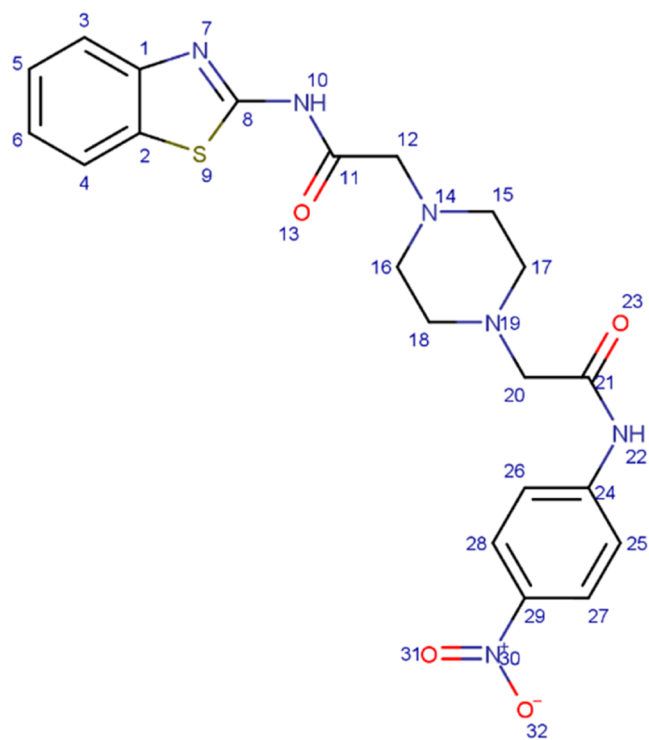
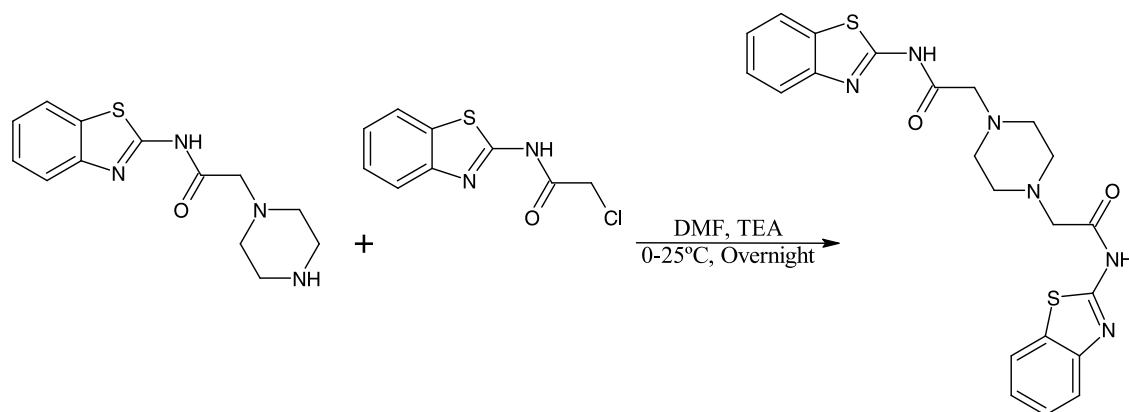


Figure 16. Chemical structure of OMS14.

thiazol-2-yl)acetamide) was an off-white powder (yield 60.2%), M.P. 327–328 °C, FT-IR (ATR): 1485, 1694, 2940, 3047, 3369 cm^{-1} , $^1\text{H-NMR}$ (400 MHz, DMSO) δ 12.99 (s, 2H, NH of N10 & N22), 4.48 (s, 4H, CH_2 of C12 & C20), 2.40–2.73 (m, 8H, CH_2 of C15, C16, C17, & C18), 7.20–8.06 (m, 8H, CH of C3, C4, C5, C6, C29, C30, C31, & C32). $^{13}\text{C-NMR}$ (400 MHz, DMSO) δ 166.43 (C11, & C21), 158.06 (C8, & C24), 148.83 (C1 & C28), 121.00–132.03 (C2, C3, C4, C5, C6, C27, C29, C30, C31, & C32), 31.24–43.03 (C12, C20, C15, C16, C17 & C18) ppm. GC-MS calculated 466.12 and found $\text{MH}^+ = 466.11$ (Figures 18, S18, S35, S67, and S68).

2.3.3. In Vitro Biological Studies. **2.3.3.1. Cell Culture and Seeding.** The A549 cancer cell line was generously supplied by Dr. Ahmad Sharab from the University of Jordan and sourced from the American Type Culture Collection (ATCC) located in Manassas, VA. The MCF-7 cell line was purchased from ATCC. The A549 and MCF-7 cancer cells were grown in Dulbecco's modified Eagle's medium or RPMI, respectively (Life Technologies, Inc., Rockville, MD), and supplemented with

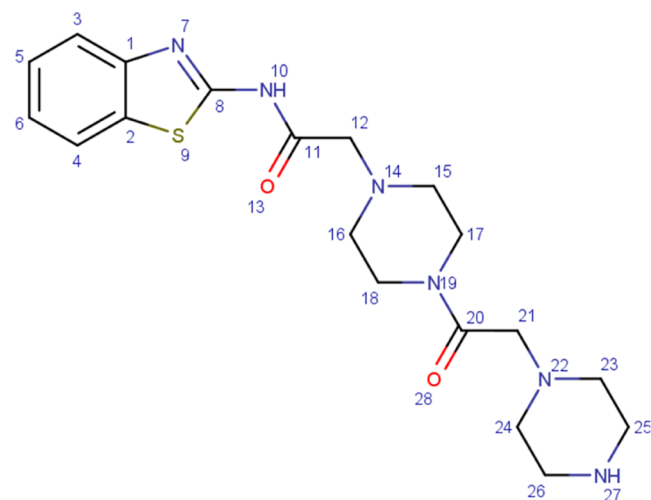


Figure 17. Chemical structure of OMS15.

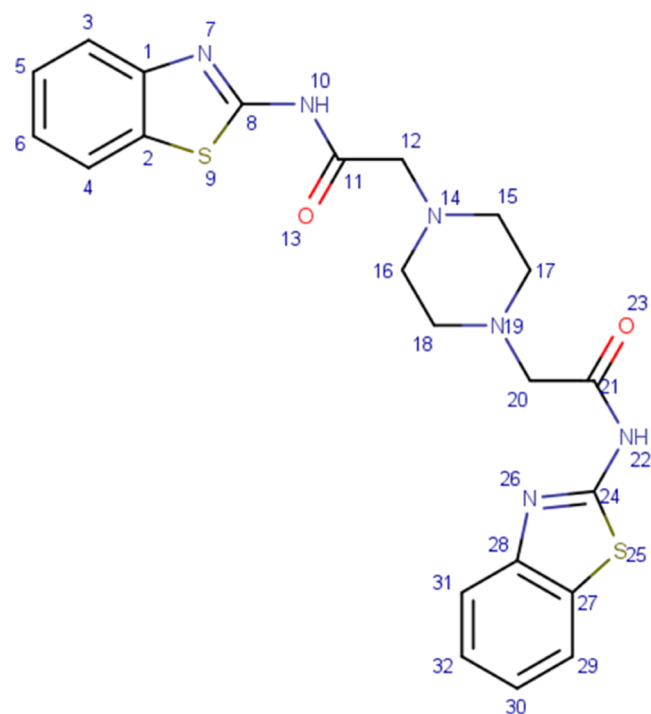


Figure 18. Chemical structure of OMS16.

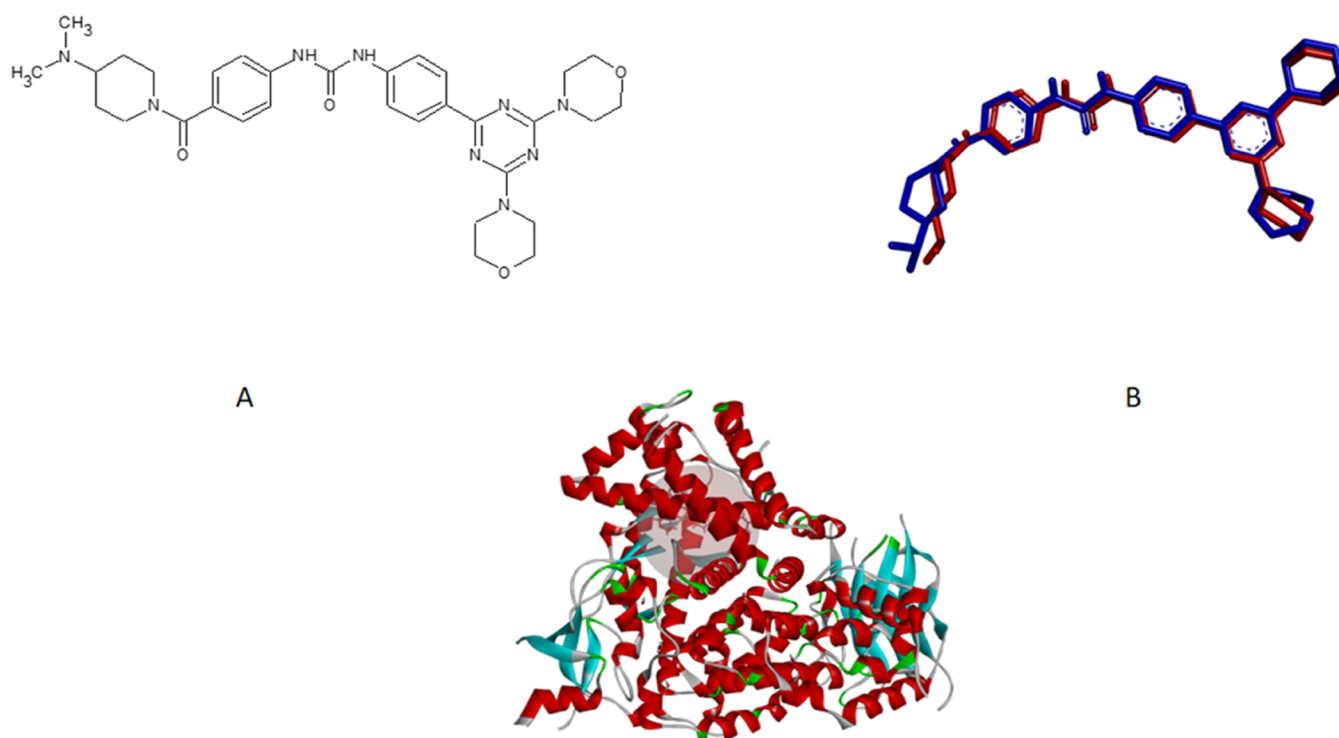


Figure 19. Gedatolisib ligand and PI3K γ protein: A: gedatolisib ligand (7JWE), cocrystallized; B: the cocrystallized conformation and the docked conformation of the cocrystallized ligand (7JWE); and C: the PI3K γ protein's binding site, represented by PDB code 7JWE.

heat-inactivated fetal bovine serum (10%; Sigma-Aldrich, St. Louis, MO), streptomycin, penicillin (1%), and glutamine (2 mmol/L). The cancer cell lines that were chosen for this study were cultivated under controlled conditions at a temperature of 37 °C and a humidity level that was maintained at a suitable level. The culture environment was supplemented with 5% CO₂. The cells were allowed to grow until they reached a recovery rate of 80%. The cancer cell lines, A549 and MCF-7, were chosen for this study and were cultured in 96-well plates at two different densities: 2000 cells per well and 10,000 cells per well, respectively. The cells were cultured for 24 h before treatment with the chemicals to facilitate cell adhesion to the well surface. Subsequently, the media underwent aspiration and were subsequently replenished with 100 μ L of fresh media containing varying concentrations of the target compounds. The cells that underwent treatment were subjected to incubation for 72 h at a temperature of 37 °C in an environment with controlled humidity and a CO₂ concentration of 5%.

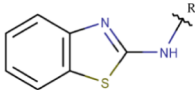
2.3.3.2. MTT Assay. The MTT experiment was conducted as described earlier³⁹ using A549 and MCF-7 cancer cell lines to evaluate the anticancer efficacy of compounds OMS1–OMS16. In summary, following a 72 h incubation period, a 20 μ L volume of a 5 mg/mL solution of (4,5-dimethylthiazol-2-yl)-2,5-diphenyltetrazolium bromide (MTT) was introduced into each well and subjected to an additional 4 h incubation at a temperature of 37 °C. Following the incubation period, the medium was subsequently extracted, resulting in the precipitation of violet formazan crystals within the wells. The formazan crystals obtained were dissolved by the addition of 100 μ L of dimethyl sulfoxide (DMSO) to each well. Subsequently, the plates were subjected to analysis using a microplate reader, namely, the GLOMAX instrument, to determine the absorbance values of the samples at wavelengths of 450 and 540 nm. Every chemical was subjected to triplicate testing in three separate tests

for each cell line. The IC₅₀ values of the most potent drugs were determined by nonlinear regression analysis using GraphPad Prism 9.3.1 software.

2.3.3.3. In Vitro PI3K γ Enzymatic Activity. The *in vitro* investigation of the biological activity of the final compounds (OMS1–OMS16) against PI3K γ was conducted using an Adapta universal kinase assay (ADP-fluorescent based immunoassay) provided by Invitrogen/Thermo Fisher Scientific. The experimental procedure consists of two distinct stages: a phase involving the activation of kinases and a subsequent phase dedicated to the detection of ADP. During the initial phase, the necessary components for the kinase reaction are introduced into the well, followed by an incubation period of 60 min. Following the completion of the reaction, an assay well is supplemented with a detection solution comprising a europium-labeled anti-ADP antibody, an Alexa Fluor 647-labeled ADP tracer, and ethylenediamine tetraacetic acid (EDTA), which serves the purpose of halting the kinase reaction. The formation of ADP by the kinase activity, in the absence of any inhibitor, will cause the displacement of the Alexa Fluor 647-labeled ADP tracer from the antibody. Consequently, this displacement will lead to a reduction in the time-resolved fluorescence resonance energy-transfer (TR-FRET) signal. When an inhibitor is present, the kinase reaction leads to a decrease in the quantity of ADP produced, causing a strong association between the intact antibody tracer and resulting in a significant TR-FRET signal. The determination of ADP formation involves the calculation of the emission ratio derived from the assay well.

2.3.3.4. Antimicrobial Activity. This study tested OMS1–OMS16 chemical compounds against Gram-positive and Gram-negative bacterial pathogens, including *Staphylococcus aureus* and *Escherichia coli*, *in vitro*. Antimicrobial tests were performed at 100 μ g/mL using the disc diffusion method. The solvent control in this investigation was dimethyl sulfoxide (DMSO),

Table 1. Synthesized Compounds (OMS1–OMS16) and Standard Inhibitors



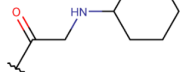
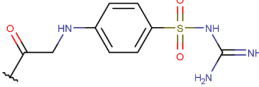
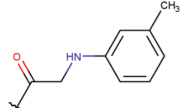
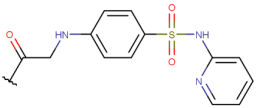
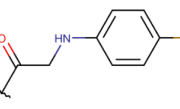
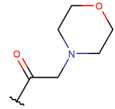
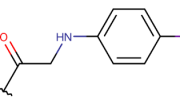
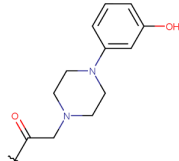
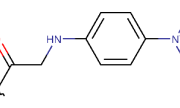
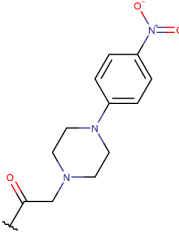
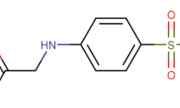
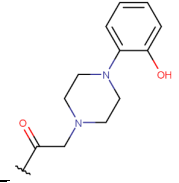
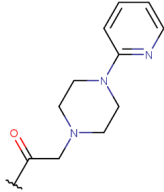
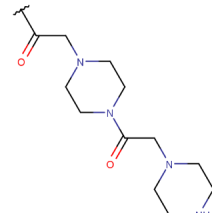
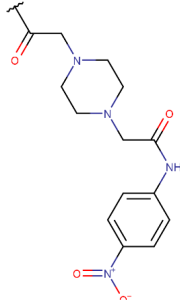
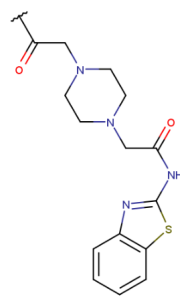
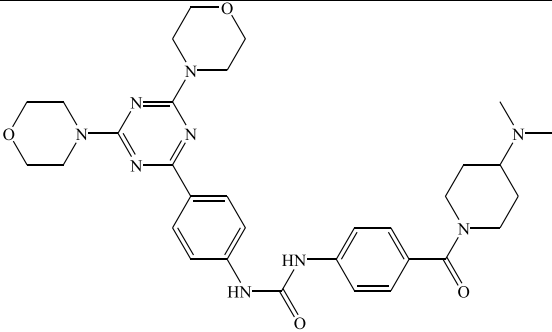
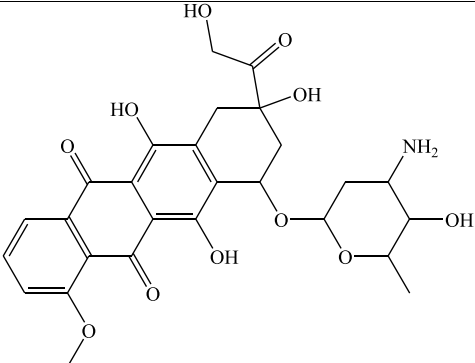
Compound	(R)	Compound	(R)
OMS1		OMS7	
OMS2		OMS8	
OMS3		OMS9	
OMS4		OMS10	
OMS5		OMS11	
OMS6		OMS12	
OMS13		OMS15	
OMS14		OMS16	

Table 1. continued

Compound	(R)	Compound	(R)
			
	Gedatolisib		
			
	Doxorubicin		

and the culture media was nutrient agar. After inoculation, the plates were incubated at 37 °C for 24 h to promote bacterial growth. Negative controls were made with DMSO, amoxicillin, ciprofloxacin, and tetracycline. The zone of inhibition against test organisms was used to evaluate antibacterial activity after incubation. This measurement was compared to the standard.

2.3.4. Molecular Modeling. 2.3.4.1. Software. 1- Biovia Discovery Studio 2021.

- 2- ChemDraw Ultra 7.0 version.
- 3- Marvin Sketch 21.18 version.
- 4- Free trial version of Mestrenova 14.2.3.
- 5- Free trial version of GraphPad Prism 9.3.1.
- 6- ACD/ChemSketch freeware version 2021.2.0
- 7- Free trial version of SpectraGryph 1.2.
- 8- GraphPad Prism 9.3.1 software.

2.3.4.2. Computational Docking. 47 compounds of 2-aminobenzothiazole conjugate (Appendix V) were created and selected for computational docking and filtration. Synthesis and biological evaluation used 16 optimum hits. The three-dimensional (3D) coordinates of the PI3K γ protein, cocrystallized with gedatolisib, were retrieved from the Protein Data Bank (PDB code: 7JWE) at a resolution of 2.55 Å.⁴⁰ The protein was generated by adding hydrogen atoms with Biovia Discovery Studio. The object was then cleansed, prepared, and restored, adding atoms, correcting connectivity and naming, and inserting loops. Figure 19 shows Biovia Discovery Studio 2021's "Define and Edit Binding Site" tool defining the active site based on the cocrystallized ligand (7JWE). Docking validation required removing the target protein's cocrystal ligand (7JWE) from the binding site. After redocking with the LibDock algorithm, the root-mean-square deviation (RMSD) was calculated to

verify the ligand postures' similarity, as shown in Figure 19. Initial ligand placement: compared to the cocrystallized stance, the posture with the greatest LibDock score had an RMSD value of 1.29 Å, below the criterion of 2 Å. This variance is permissible.⁴¹ A list of 16 2-aminobenzothiazole compounds with unique moieties was docked at the PI3K γ protein binding site (PDB code: 7JWE, resolution: 2.55 Å)⁴⁰ using the default LibDock algorithm. One compound with two amino benzothiazoles and the other with two piperazines had the highest LibDock score among compounds with 2-amino benzothiazoles.

2.3.4.3. Absorption, Distribution, Metabolism, Excretion, and Toxicity (ADMET) Prediction. ADMET experiments used Biovia Discovery Studio 2021, and structures were designed with ACD/ChemSketch Freeware 2021.2.0. The default Biovia Discovery Studio 2021 (ADME) settings for absorption, distribution, metabolism, and excretion were used to analyze the structures of the synthesized compounds (OMS1–OMS16) (Table S2). After including all necessary data, the chemicals were analyzed using the TOPKAT model toxicity function (Table S3).

2.3.4.3.1. ADMET: Human Intestinal Absorption. For oral delivery, this model predicts human intestinal absorption (HIA). Unlike blood–brain penetration, intestine absorption is measured by percentage rather than concentration. Well-absorbed chemicals can be absorbed into the bloodstream at least 90%. The ADMET_PSA_2D and ADMET_AlogP98 planes have ellipses for 95% and 99% confidence intervals in the intestinal absorption model, respectively.⁴²

Ellipse locations are expected to have well-absorbed compounds. The 95 and 99% ellipses are expected to include 95 and 99% of well-absorbed substances, respectively. Intestinal

absorption prediction has four levels: User Guide, Biovia Software classifies ratings as 0 (Good), 1 (Moderate), 2 (Poor), and 3 (Very Poor).⁴²

2.3.4.3.2. ADMET: Aqueous Solubility. Linear regression was employed in this model to estimate the solubility of each drug in water at a temperature of 25 °C.

2.3.4.3.3. Blood–Brain Barrier. This model predicts the blood–brain barrier (BBB) permeability after oral delivery. The ADMET_PSA_2D and ADMET_AlogP98 planes have 95 and 99% confidence ellipses, respectively. It also forecasts blood–brain penetration using quantitative linear regression. The ellipses in this context are different from those in the ADMET—human intestinal absorption—despite their identical connotation. The prediction levels inside the confidence ellipsoids of 95% and 99% are 0 (extremely high penetrant level), 1 (high), 2 (medium), and 3 (low).

2.3.4.3.4. The Hepatotoxicity Model. The hepatotoxicity model predicts organ toxicity for several structurally different medications. The sentence “True denotes hepatotoxicity, while False indicates the absence of hepatotoxicity”.⁴³

2.3.4.3.5. NCI 60-Cell One-Dose Screen. We conducted the evaluation of our compounds in collaboration with the National Cancer Institute (NCI) as part of their comprehensive testing program. After our compounds were submitted to NCI, they underwent thorough evaluation using the NCI’s established protocols. The testing procedures were conducted by NCI’s standards, which can be found on their official website (www.cancer.gov).

3. RESULTS AND DISCUSSION

3.1. Chemistry. Synthesis of 2-chloro-*N*-(benzothiazol-2-yl)acetamide from 2-aminobenzothiazole and chloroacetyl chloride in triethylamine yielded P1 (Figures 2, S19, S36, S69, and S70). Triethylamine was used as a catalyst.⁴⁴ Table 1 shows (OMS1–OMS16) and standard inhibitors; the early compounds (OMS1–OMS13) were generated by nucleophilic substitution of monochloroacetyl chloride’s chlorine atom with various amines.^{45–47} In monochloroacetyl chloride, acid chloride is highly reactive because the carbonyl carbon is linked to oxygen and chlorine, making it electron-deficient and vulnerable to nucleophile attack. The chlorine atom also leaves well. Alkyl chloride carbon has limited nucleophilic substitution reactivity. Acid chloride’s chlorine atom is usually substituted at low temperatures. Depending on the nucleophile’s reactivity, alkyl chloride’s second chlorine atom may be substituted at high temperatures. The chemicals OMS1, OMS2, and OMS9 were synthesized by reacting cyclohexylamine, *m*-toluidine, and morpholine with 2-chloro-*N*-(benzothiazole-2-yl)acetamide (P1) at temperatures from 75 to 100 °C using standard methods. The final reaction mixture was recrystallized using acetone/water antisolvent to purify OMS9.

The solvent-free/neat fusion approach was used to react 2-chloro-*N*-(benzothiazol-2-yl)acetamide (P1) with chosen amines (*p*-fluoroaniline, *p*-iodoaniline, *p*-nitroaniline, sulfanilamide, sulfaguanidine, and sulfapyridine) to create sufficient OMS3–OMS8 chemicals.^{48,49}

Substituted piperazines—3-(1-piperazinyl)phenol, 1-(4-nitrophenyl)phenol, 2-(1-piperazinyl)phenol, and 1-(2-pyridyl)phenol—reacted with 2-chloro-*N*-(benzothiazol-2-yl)acetamide (P1) at a reflux temperature in DMF to yield compounds (OMS10–OMS13). The conventional method for nucleophilic substitution of substituted anilines and sulfa-amine with 2-chloro-*N*-(benzothiazol-2-yl)acetamide (P1) failed at temper-

atures from 25 to 160 °C, using solvents with high boiling points. Sulfa-amine and substituted anilines have weak nucleophilicity, which explains their failure. To synthesize molecules OMS3–OMS8 in high yields, a solvent-free/neat fusion process was used at temperatures near 200 °C.

The second stage involved linking 2-aminobenzothiazole–piperazine with monochloroacetyl chloride. 2-Chloro-*N*-(benzothiazol-2-yl)acetamide (P1) was reacted with piperazine (Scheme 3) and acetone/water mixture at 60 °C, RPM 150, to produce *N*-(1,3-benzothiazol-2-yl)-2-(piperazine-1-yl)acetamide (P2). P2 then reacted with 4-nitroaniline, piperazine, and 2-aminobenzothiazole (Schemes 6–8), respectively, using conventional methods at different temperatures (50 °C).

Using ¹H, ¹³C, and IR investigations, the synthesized 2-aminobenzothiazole derivative compounds (OMS1–OMS16) and intermediate P1 were characterized. The appendices show that mass spectrometry (GC-MS) analyses verified the products’ production.

FT-IR analysis of compounds OMS1–OMS16 (Appendix I) revealed NH and C=O groups at absorptions of 3270–3360 and 1557–1680 cm⁻¹, respectively. The absorptions at 3200–3400 show the OH group in OMS10 and OMS12. Both aromatic and aliphatic C–H stretch vibrations are confirmed by the bands at 3060–3140 and 2845–2935 cm⁻¹. N=O and group absorptions at 1500–1660 and 1260–1390 cm⁻¹ are connected in compounds OMS5, OMS11, and OMS14. Some chemicals’ FT-IR spectra are wide and interfere with peaks due to undesired water in the end products.

In ¹H-NMR analysis, all aromatic and aliphatic H atoms were identified in their predicted locations (Appendix III). The absorption of aromatic H atoms of unsaturated benzene rings in benzothiazole, substituted amines, and piperazines was 6.6–8.2 ppm. NH of aminobenzothiazole showed a wide singlet at 10–12 ppm. The saturated benzene ring of piperazine in derivatives OMS10–OMS14 has H atoms at 2.0–3.5 ppm. The ¹H-NMR spectra exhibited recognizable peaks for the produced derivatives.

All carbon atoms were in their predicted areas in ¹³C-NMR spectra (Appendix III). Carbon atom absorption in the C=O group was 165–170 ppm. At 37–42 ppm, aliphatic CH₂ carbon emerged. The aromatic carbon atoms of benzothiazole amines and piperazines were at 115–135 ppm. Compound identities were validated by mass analysis (Appendix II). All synthesized derivatives have expected molar masses (*m/z*).

3.2. In Vitro Biological Studies. Thermo Fisher Scientific evaluated the resulting compounds (OMS1–OMS16) for anti-PI3Kγ activity at 100 μM (Table 2). The most effective synthetic compounds against PI3Kγ were OMS1 and OMS2, with 47 and 48% inhibition rates, respectively, and they were also tested against other kinase enzymes: Akt1, Akt3, CDK1, PDK1, PI3Kα, PI3Kδ, and PKN2 (Table 3). At a dose of 100 μM, the remaining drugs showed minimal action or inhibition. *In vitro* MTT testing was used to examine the anticancer activity of compounds (OMS1–OMS16) against MCF-7 and A549 cancer cell lines (Table 4). IC₅₀ values of the most potent compound OMS14 were 22.13 and 26.09 μM against MCF-7 and A549 cancer cell lines, respectively, as shown in Table 5. The graphical presentation of the dose–inhibition relationship is illustrated in Figure 20.

Gedatolisib, a potent PI3Kγ inhibitor,⁵⁰ and doxorubicin, a potent chemotherapeutic medicine,⁵¹ were used as positive controls in the MTT assay study.

Table 2. Anti-PI3K γ Activity of Compounds OMS1–OMS16^b

compound ID	% of inhibition against PI3K γ enzyme at a concentration of 100 μ M		% of inhibition (mean)
	point 1	point 2	
OMS1	54	40	47
OMS2	44	52	48
OMS3	20	28	24
OMS4	0	0	0
OMS5	0	0	0
OMS6	3	22	13
OMS7	29	22	25
OMS8	0	0	0
OMS9	0	3	2
OMS10	3	0	2
OMS11	6	0	3
OMS12	28	4	16
OMS13	–2	8	3
OMS14	15	24	19
OMS15	0	0	0
OMS16	2	0	1
Staurosporine ^a	100	98	99

^aPositive control with reported IC₅₀ = 1.0 nM.⁶⁵ ^bNumber of trials = 2, RSD < 5%.

Table 3. Kinase Selectivity for Compound OMS14^a

enzyme	% of inhibition of compound OMS14 against different enzymes at concentration 100 μ M		% of inhibition (mean)
	point 1	point 2	
AKT1 (PKB α)	11	17	14
AKT3 (PKB γ)	27	29	28
CDK1/cyclin B	23	25	24
PDK1 Direct	–6	–8	–7
PIK3CA E542 K/PIK3R1 (p110 α E542 K/p85 α)	33	36	34
PIK3CD/PIK3R1 (p110 δ /p85 α)	66	64	65
PKN2 (PRK2)	11	8	10

^aNumber of trials = 2, RSD < 5%.

The most active compounds against MCF-7 and A549 cancer cells were OMS14 and OMS5. Active compounds with 4-nitroaniline structures showed considerable inhibition against cancer cell lines at 100 and 50 μ M doses. The IC₅₀ values of the substances ranged from 22.13 to 61.03 μ M. OMS14 (Figure 20), which has high efficacy against breast and lung cancer cell lines, has minimal activity against the PI3K γ enzyme, suggesting a different mechanism of action for its anticancer effects. Testing against cancer enzymes other than PI3K γ , Akt1, Akt3, CDK1, PDK1, PI3K α , PI3K δ , and PKN2 revealed moderate action (65% inhibition) against PIK3CD/PIK3R1 (p110 δ /p85 α), suggesting a potential mechanism of anticancer activity.

OMS5 compounds showing anticancer effectiveness against breast and lung cancer cell lines lack PI3K γ enzyme activity, suggesting other modes of action. Several studies introduced various 2-aminobenzothiazole derivatives as anticancer drugs, suggesting another mode of action. The above chemicals

Table 4. Inhibition Percentage of Synthetic 2-Aminobenzothiazole Derivatives against A549 and MCF-7 in MTT Assay^b

cpd.	experimental % of inhibition on MCF-7 and A549 cancer cell line at (100 μ M) concentration	
	A549	MCF-7
OMS1	1.72	34.44
OMS2	3.73	–6.5
OMS3	2.80	18.31
OMS4	–2.32	30.84
OMS5	64.15	32.01
OMS6	39.64	–8.74
OMS7	–3.59	10.19
OMS8	11.21	15.06
OMS9	17.16	2.74
OMS10	38.12	4.5
OMS11	21.98	35.03
OMS12	48.51	54.08
OMS13	26.86	53.07
OMS14	90.59	85.05
OMS15	56.69	–23.63
OMS16	56.62	5.23
Dox. ^a	82.23	

^aDoxorubicin is a potent anticancer drug as a standard. ^bNumber of trials = 3, RSD < 5%.

Table 5. IC₅₀ of OMS5 and OMS14 against A549 and MCF-7^c

cell line	A549			MCF-7		
	IC ₅₀ (μ M)	Hill slope	R ²	IC ₅₀ (μ M)	Hill slope	R ²
OMS5	61.03	0.49	2.00	ND		
OMS14	26.09	0.49	2.00	22.13	1.30	0.94
Gedatolisib ^a	16.46	2.68	0.96	13.06	1.982	0.99
Doxorubicin ^b	16.61	2.21	0.98	ND		

^aPositive control as an anticancer agent with selective kinase inhibition. ^bPositive control as an anticancer agent. ^cNumber of trials = 2, RSD < 5%.

suppress CDK2, mTOR, AKT, p42/44 MAPK, and EGFR to fight cancer.

The study found that the IC₅₀ values for doxorubicin and gedatolisib were 16.61 and 16.46 μ M against A549 cancer cell lines (Table 5), respectively, while the reported IC₅₀ for gedatolisib was 9.05 μ M.^{52,53} The reported IC₅₀ for doxorubicin against A549 was 0.071 μ M.^{54–56} The most active synthesized compound (OMS14) was tested against cancer enzymes other than PI3K γ , and the result is shown in Table 3.

The synthesized compounds (OMS1–OMS16) were tested against *S. aureus* and *E. coli* *in vitro*. Table 6 shows that several derivatives, including OMS1, OMS3, OMS4, OMS10, OMS12, and OMS14, have action against Gram-positive *S. aureus*, especially OMS1, which has a diameter of inhibition of 22 mm equivalent to amoxicillin. The results may be used as templates for further modifications or derivatization to create more effective antibacterial medicines.

3.3. Computational Docking and PI3K γ Enzymatic Activity. Figure 21 depicts the interaction between the gedatolisib ligand (VL11201) and the docked OMS14 with the ATP binding site of PI3K γ protein (PDB code: 7JWE).⁴⁰

Table 7 displays the LibDock score, hydrogen bonds, and a two-dimensional schematic of the compounds' spatial arrange-

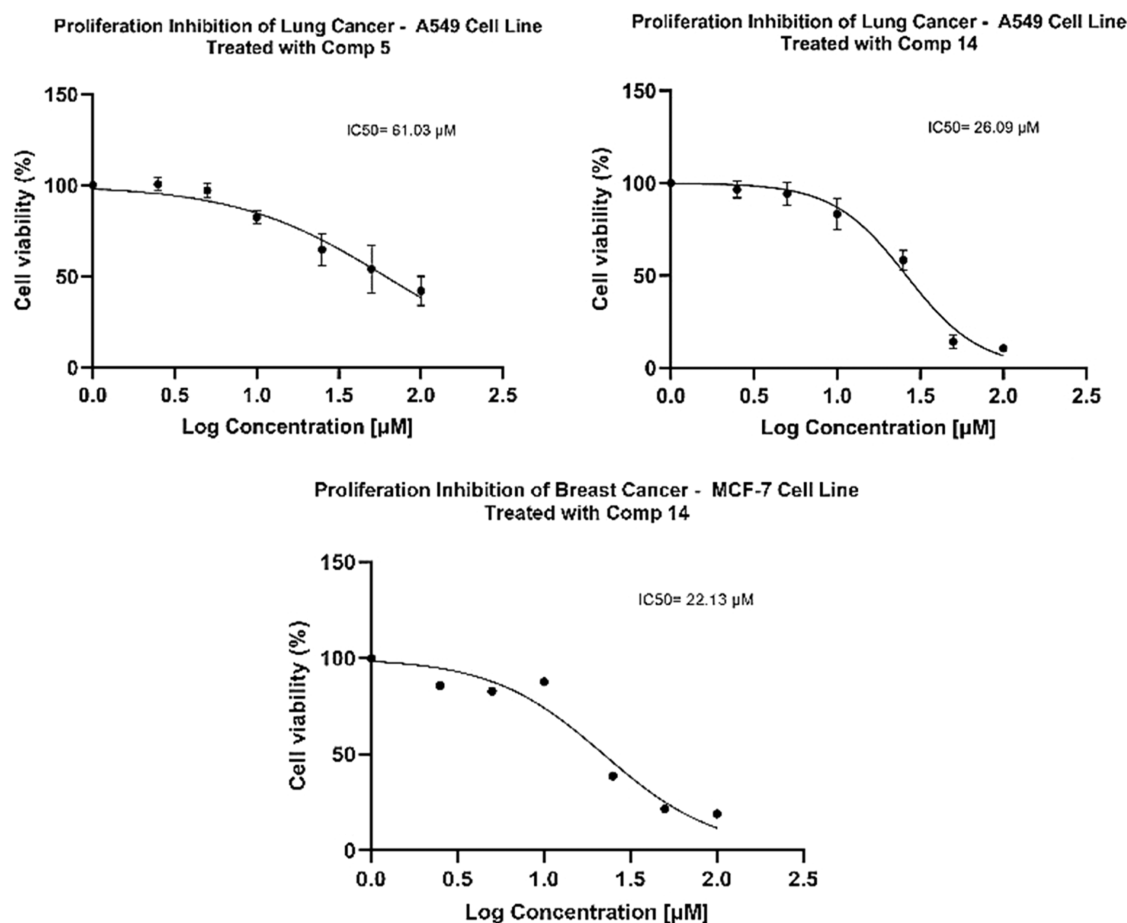


Figure 20. Cell viability of OMS5 against A549, and OMS14 against A549 and MCF-7 cell lines.

Table 6. Antimicrobial Activity of Synthesized Derivatives^c

compound	Gram-positive bacteria		Gram-negative bacteria	
	<i>S. aureus</i>		<i>E. coli</i>	
OMS1	22		0	
OMS2	0		0	
OMS3	15		0	
OMS4	10		0	
OMS5	0		0	
OMS6	0		0	
OMS7	0		0	
OMS8	0		0	
OMS9	0		0	
OMS10	11		0	
OMS11	0		0	
OMS12	20		0	
OMS13	0		0	
OMS14	15		0	
OMS15	0		0	
OMS16	0		0	
Amoxicillin ^a	22		20	
Ciprofloxacin ^a	0		25	
Tetracycline ^a	25		0	
DMSO ^b	0		0	

^aPositive control. ^bNegative control. ^cNumber of trials = 3, RSD < 5%.

ment in the PI3K γ enzyme binding site (PDB: 7JWE). Computational docking determines the best orientation and

conformation for a tiny molecule, usually a drug candidate, to bind to a bigger receptor molecule, usually a protein. It aims to create a stable complex molecule.⁵⁷ Computer-assisted drug discovery relies on molecular docking to predict the main binding mode(s) between a ligand and a protein with a well-defined three-dimensional structure.⁵⁸ The LibDock algorithm, created by Diller and Merz,⁵⁹ uses protein binding site features to aid docking. The protein used and the similarity between the cocrystallized ligand and the ligands being evaluated can affect the docking's capacity to distinguish chemical compounds and decoys.⁶⁰

Based on the provided information, the protein data bank file (7JWE, 2.55 Å resolution)⁴⁰ was accessed for the intended purpose. We report the structural data of the PI3K γ protein complexed with gedatolisib ligand (VL11201) obtained through cocrystallization. The docking approach was validated using the position conformation with the highest LibDock score (81.11). Using the root-mean-square deviation (RMSD) approach, the variance between the best position and the original cocrystallized pose was estimated as 1.29 Å. This value is below 2 Å, showing good agreement between the two positions. As in Figure 21, the cocrystallized ligand (VL11201) binds to the PI3K γ enzyme's binding site (7JWE).⁴⁰ The protein's amino acid residues connect via four hydrogen bonds: At 2.53 Å, valine 882 forms a hydrogen bond with oxygen (O). At 3.30 Å, threonine 887 forms a hydrogen bond with oxygen (O). Aspartic acid 841 forms hydrogen bonds with NH₂ at 1.87 and 1.77 Å distances. Table 7 shows that all synthesized drugs fit the active

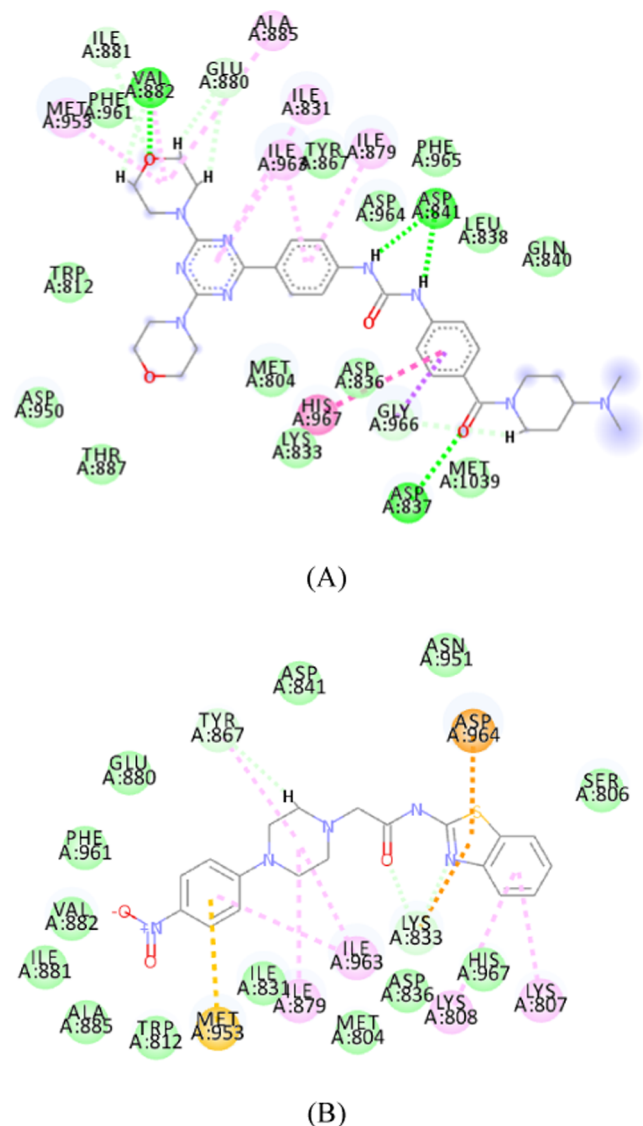


Figure 21. (A) A two-dimensional schematic representation of the interaction of the cocrystallized ligand, VL11201. (B) The OMS14 docked within the ATP binding site of PI3K γ PDB code: 7JWE, resolution = 2.55 Å.

site of the PI3K γ enzyme and have a strong LibDock score, indicating inhibition efficacy.

Table 7 shows that all synthesized derivatives outperform the cocrystallized ligand in LibDock. The chosen derivatives create 2–5 hydrogen bonds, suggesting they may be more active than the cocrystallized gedatolisib inhibitor. Compound OMS1 (LibDock score: 113.524) and compound OMS2 (LibDock score: 121.194) as the most effective against PI3K γ enzyme, with 47 and 48% inhibitions, respectively. The synthesized compounds showed low to no efficacy against cancer cell lines at 100 μ M dose. The low connection between docking results and *in vitro* enzymatic activity shows many LibDock algorithm shortcomings. The site feature approach (LibDock) prioritizes library selection above compound ranking by efficiently docking combinatorial libraries.⁵⁹ However, scoring functions vary widely between protein systems, and predictions often do not match results.⁶¹ Predicting protein–ligand affinity is a major computational chemistry difficulty.⁶²

Table 7. LibDock Score and Hydrogen Bonds of the Synthesized Derivatives into PI3K γ Enzyme Binding Sites^a

compound	LibDock score	no. of H-bonds	H-bonds (cpd part–amino acid)	bond length distance (Å)
OMS1	113.524	5	N–ASP a:964	2.39
			NH–ASP a:964	2.51
			NH–ASP a:841	1.96
			CH–ASP a:841	2.08
			O–LYS a:833	2.76
OMS2	121.194	5	N–ASP a:964	4.63
			NH–ASP a:964	4.17
			NH–ASP a:841	4.35
			CH–ASP a:841	3.85
			O–LYS a:833	4.96
OMS3	117.915	2	O–LYS a:833	4.95
			NH–ASP a:841	4.45
OMS4	112.952	2	NH–ASP a:841	4.58
			O–ASP a:964	3.58
OMS5	123.488	3	NH–ASP a:841	4.44
			O–ASP a:964	3.98
			O–ASP a:837	4.00
OMS6	126.434	5	NH–GLU a:880	4.77
			O–LYS a:833	5.06
			CH–ASP a:841	5.13
			NH–ASP a:841	3.67
			S–HIS a:967	3.02
OMS7	123.894	2	NH–VAL a:882	4.06
			NH–ASP a:836	5.27
OMS8	128.688	3	O–ASP a:837	3.91
			NH–ASP a:841	4.30
			S–ASP a:964	4.75
OMS9	105.176	3	NH–VAL a:882	3.01
			NH–GLU a:880	4.92
			NH–TYR a:867	3.51
			CH–TYR a:867	6.00
			N–HIS a:967	4.14
OMS10	133.31	2	CH–TYR a:867	5.36
			O–LYS a:833	4.51
			N–LYS a:833	5.77
OMS11	109.058	3	CH–TYR a:867	5.40
			N–HIS a:967	4.01
OMS12	128.368	2	N–HIS a:967	4.10
			CH–TYR a:867	6.25
			CH–ASP a:841	5.03
OMS13	134.458	3	O–LYS a:833	4.73
			N–LYS a:833	5.50
			O–LYS a:833	5.22
OMS14	138.055	3	CH–TYR a:867	5.64
			CH–TYR a:867	5.52
			S–ASP a:837	3.86
OMS15	153.032	5	O–HIS a:967	4.72
			NH–TYR a:867	3.45
			NH–ASP a:841	4.30
			CH–ASP a:841	4.87
			CH–ASP a:841	4.87

^aLibDock is a docking tool with Biovia 2022.

3.4. ADMET Prediction of Synthetic Compounds (OMS1–OMS16). ADMET calculated absorption, water solubility, blood–brain barrier, atom-based Log P98 (A Log P98), two-dimensional (2D) polar surface area (ADMET 2D PSA), and hepatotoxicity prediction based on the molecular

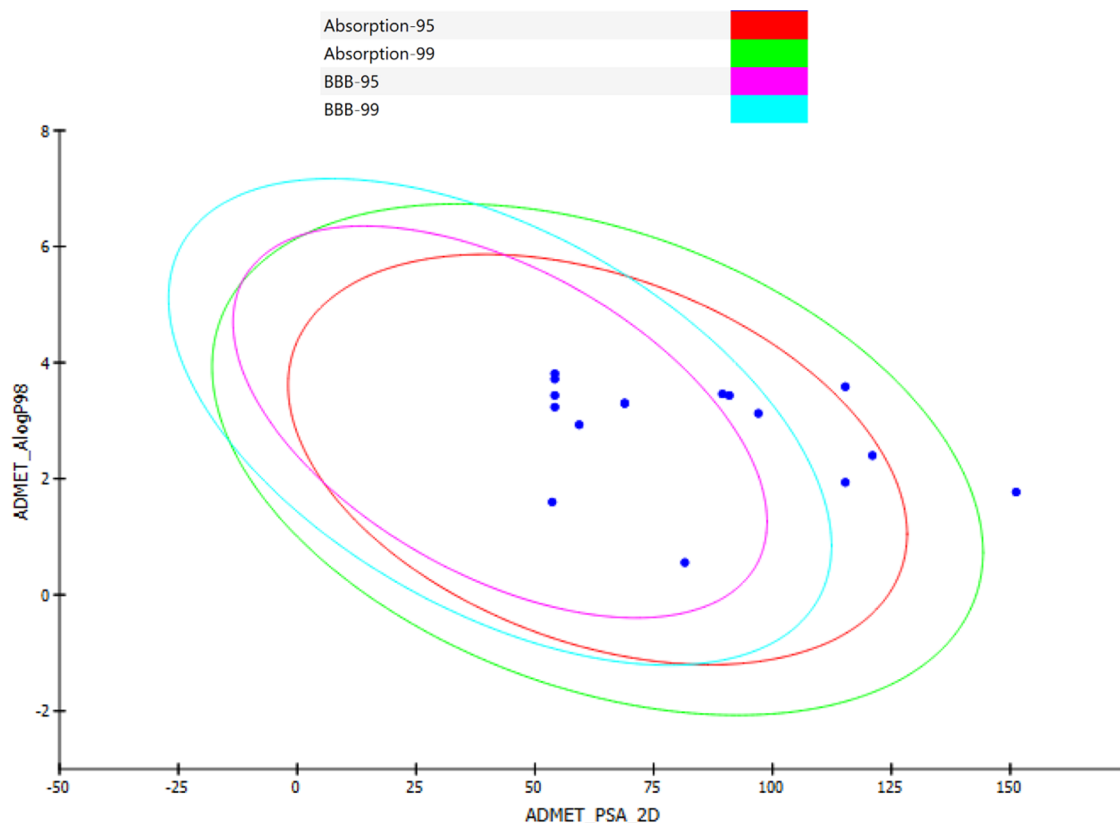


Figure 22. Pharmacokinetic properties for synthesized derivatives.

chemical structure. Calculations were done with Biovia Discovery Studio 2021.

The ADMET plot compounds have BBB values from 1 to 4, suggesting high to very low blood–brain barrier permeability. The chemicals OMS14 and OMS5 have low to extremely low blood–brain barrier (BBB) permeability, suggesting they could treat non-CNS tumors. 88% of substances, including OMS5 and OMS14, had absorption levels of 0, suggesting good human intestinal absorption. Only compound OMS6 had moderate absorption; none had low absorption. The majority of chemicals have ADME aqueous solubility levels between 2 and 3, indicating good solubility. Drug bioavailability is linked to polar surface area (PSA). Thus, compounds with passive absorption and $PSA \leq 140$ have lower bioavailability. Thus, all synthesized compounds except OMS6 should have good passive oral absorption. The PSA_{2D} and $A \log P_{98}$ characteristics were used to create a 2D ADMET graphic (Figure 22). Passive absorption and decreased bioavailability characterize molecules with PSA values below 140. The polar surface area (PSA) ranged from 53.654 to 121.011 for the chemicals studied. This range shows significant passive oral absorption for these drugs.

Figure 22 displays a 2D plot of the expected pharmacokinetic parameters for synthetic 2-aminobenzothiazole derivatives (OMS1–OMS16). The blue dots represent the investigated drugs, the y -axis represents atom-based $\log P_{98}$, and the x -axis represents 2D polar.

According to our ADMET investigation, all 2-aminobenzothiazole derivatives (OMS1–OMS16) except OMS6 are good medication candidates for modifying new hits as anticancer agents.⁶³ Biovia Discovery Studio 2021 software predicts acceptable pharmacokinetic characteristics and toxicity, promising new medication candidates.

3.5. NCI 60-Cell Line Inhibition Measurement. The NCI 60 (National Cancer Institute 60) cell line panel is a collection of 60 diverse human cancer cell lines, representing nine different cancer types.⁶⁴ These cell lines are extensively used in cancer research, drug discovery, and development. Inhibition measurements in the context of NCI 60 typically refer to the evaluation of the effect of a particular compound or treatment on the growth or viability of these cancer cell lines.

The compounds OMS5 and OMS14 are further analyzed on 60 different cell lines through NCI services given the NCI codes 848880 and 848881, respectively, and found active as shown in Table 8 and Figure 23. The percentage of inhibition is shown in Figures S1 and S2 in the Supporting Information.

Table 8 shows the following values: GI_{50} represents the concentration of a drug that reduces total cell growth by 50%, IC_{50} stands for inhibitory concentration at 50%, LC_{50} stands for the 50% lethal concentration, TGI represents the necessary concentration (μM) for total inhibition of cancer cell proliferation. The results show submicromolar inhibition of OMS5 and OMS14 on colon cancer, renal cancer, CNS cancer, ovarian cancer, melanoma, and leukemia with GI_{50} ranged from 0.36 to 2.3 μM and 0.66 to 3.02 μM , respectively; the IC_{50} values also show a similar pattern of activity ranging from 0.44 to 12.0 μM and 0.81 to 9.1 μM respectively. This indicates the potential and promising activity of both OMS5 and OMS14 as a broad-spectrum anticancer agent with acceptable drug-like properties with low toxicity and high selectivity.

To confirm the safety of the synthetic compounds OMS5 and OMS14, we screened them on normal cell lines (Fibro cells). It was found that there is toxicity at 100 μM , which is considered a high concentration, so, we tested the compounds at 10 μM to

Table 8. NCI 60-Cell Line Inhibition Measurement for Compounds OMS5 and OMS14^a

panel name	cell name	cell line inhibition of compound OMS5 (μM)				cell line inhibition of compound OMS14 (μM)			
		GI ₅₀	IC ₅₀	LC ₅₀	TGI	GI ₅₀	IC ₅₀	LC ₅₀	TGI
breast cancer	BT-549	2	5.4	27.5	6.5	3.0	7.8	36.3	9.8
	HS 578T	1.6	5.9	93.3	5.6	2.4	8.9	100	8.5
	MCF-7	0.4	0.5	74.1	10	2.8	4.1	61.7	7.8
	MDA-MB-231/ATCC	1	2.3	8.3	2.9	1.9	3.9	18.2	4.7
	MDA-MB-468	0.4	1.8	5.3	1.8	1.5	3.2	7.1	3.2
	T-47D	1	4.6	74.1	4.6	2.2	5.6	100	5.8
CNS cancer	SF-268	1.3	3.5	51.3	6.6	2.2	4.6	43.7	7.1
	SF-295	0.7	1.4	24	4.4	2.2	3.7	28.8	7.1
	SF-539	0.5	1.4	6.5	2.1	2.0	4.3	20.0	5.5
	SNB-19	1	2.6	95.5	10	2.8	4.9	100	12.3
	SNB-75	1.4	3	5.9	2.9	2.0	6.6	24.0	6.0
	U251	0.9	1.7	41.7	12	2.6	3.5	50.1	11.0
colon cancer	COLO 205	0.4	0.7	4.7	1.5	1	1.7	5.0	2.2
	HCC-2998	0.9	1.6	5.3	2.2	1.7	3.1	8.9	3.9
	HCT-116	0.4	0.4	45.7	11	0.7	0.8	52.5	10.5
	HCT-15	0.5	0.7	28.8	3.7	1.7	2.8	7.9	3.7
	HT29	0.5	0.7	8.1	2.1	1.3	2.1	10.2	3.6
	KM12	1.2	2.5	52.5	12	2.9	4.5	74.1	13.5
leukemia	SW-620	0.5	0.7	43.7	7.2	0.8	1.1	87.1	5.9
	CCRF-CEM	0.9	2.3	100	50	2.5	4.0	100	17.4
	HL-60(TB)	0.8	2.5	100	14	2.5	4.4	81.3	7.6
	K-562	0.5	0.6	100	100	2.6	3.0	100	100
melanoma	MOLT-4	0.4	0.6	100	12	1.1	2.5	100	9.5
	LOX IMVI	0.6	1	8.7	2.6	1.6	2.8	6.2	3.2
non-small cell lung cancer	M14	0.9	1.4	6.5	2.5	1.7	3.0	8.3	3.8
	MALME-3M	1.1	2.1	5.0	2.3	3.0	6.6	35.5	9.3
	MDA-MB-435	0.7	1.3	4.8	2	1.8	3.0	15.1	4.6
	SK-MEL-2	1.3	3	6.3	2.8	1.8	3.5	6.9	3.5
	SK-MEL-28	1.6	3	6.9	3.3	2.1	4.0	23.4	6.2
	SK-MEL-5	1.6	2.9	5.5	3	1.7	3.2	6.3	3.3
	UACC-257	1.3	2.5	6.3	2.8	2.1	4.2	11.7	4.7
	UACC-62	1.1	2	5.5	2.5	1.7	3.1	6.9	3.5
	AS49/ATCC	0.8	1.5	100	28	1.9	3.2	100	4.6
	EKVX	1.1	2.5	26.9	4.2	2.0	3.8	27.5	4.9
ovarian cancer	HOP-62	1.2	3	25.1	4.9	1.7	3.2	8.3	3.7
	HOP-92	2.3	12	63.1	10	2.3	9.1	89.1	8.3
	NCI-H226	0.6	3	100	4.9	1.4	3.5	100	4.2
	NCI-H23	1	2.1	7.8	2.8	1.6	3.2	8.9	3.8
	NCI-H322M	1.1	2.5	28.8	4.1	1.9	3.7	40.7	5.5
	NCI-H460	0.4	0.5	39.8	3.3	1.3	1.8	21.9	4.1
	NCI-H522	0.7	2.1	6.3	2.3	1.5	3.0	6.5	3.2
	IGROV1	0.8	1.8	100	12	1.9	3.3	47.9	4.6
	NCI/ADR-RES	0.6	1.3	53.7	4.6	1.3	2.4	7.8	3.2
	OVCAR-3	1.9	4	100	9.1	2.3	4.3	100	6.6
prostate cancer	OVCAR-4	1	3	40.7	5.1	2.4	5.2	75.9	8.3
	OVCAR-5	1	2.5	46.8	5.4	1.5	3.2	57.5	4.8
	OVCAR-8	0.6	0.9	100	22	1.4	2.4	100	4.3
	SK-OV-3	1.3	5.2	100	6.8	2.2	6.6	100	8.1
renal cancer	DU-145	0.8	1.8	52.5	12	2.2	3.5	38.9	7.9
	PC-3	1.6	2.8	100	45	3.0	4.4	100	20.9
renal cancer	786-0	0.5	0.9	43.7	12	2.1	3.3	43.7	11.5
	A498	1.4	7.2	28.8	6.5	1.7	3.8	7.9	3.7
	ACHN	0.4	0.8	33.1	8.5	1.1	2.1	22.9	4.4
	CAKI-1	0.4	0.9	32.4	9.5	0.9	2.0	16.2	3.6
	SN12C	0.6	1.5	57.5	4.9	1.9	3.5	100	5.4
	TK-10	1.5	10	100	15	2.2	6.2	100	7.1
	UO-31	0.5	1.3	26.9	3.8	1.3	2.5	8.5	3.3

^aGI₅₀ represents the concentration of a drug that reduces total cell growth by 50%. IC₅₀ stands for inhibitory concentration at 50%. LC₅₀ stands for the 50% lethal concentration. TGI represents the necessary concentration (μM) for total inhibition of cancer cell proliferation.

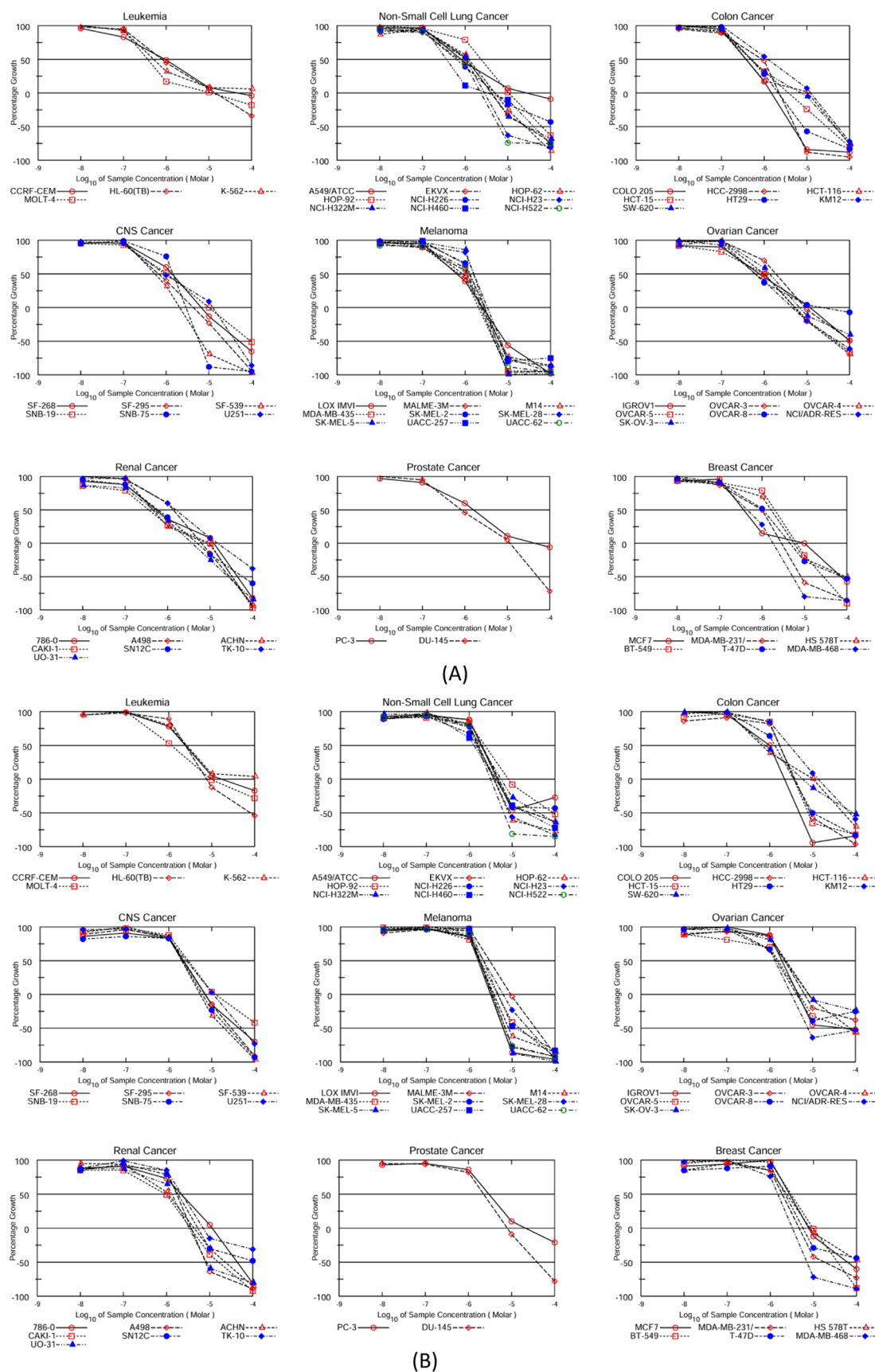


Figure 23. %Growth vs Log Conc. For compounds (A) OMS5 and (B) OMS14.

evaluate the safety of the compounds on the normal cell line as shown in Table 9.

The % inhibition of compounds of the synthetic compounds on the normal cell line is variable with potential inhibition of

Table 9. % Inhibition of Synthetic Compounds OMS1–OMS16 on Fibro Cell Line^a

compound number	%inhibition at 100 μ M	%inhibition at 10 μ M
OMS1	13	0.85
OMS2	17.7	9.09
OMS3	63.8	10.3
OMS4	27.6	1.32
OMS5	67.1	57.9
OMS6	62.7	1.52
OMS7	16.4	1.88
OMS8	43.3	8.62
OMS9	3.11	11.8
OMS10	44.1	15.9
OMS11	19.2	21.3
OMS12	22.2	24.3
OMS13	13.8	21.1
OMS14	70.5	49.4
OMS15	70	34.8
OMS16	70.1	53.8
Sorafenib	26.28	10.7

^aTrial number = 3, RMSD < 5%.

compounds OMS5 and OMS14, which indicates the toxicity of the highest active compounds on the normal cell line, although the effect is higher on the cancerous cell line, which indicates a margin of safety of OMS5 and OMS14. However, for further development of synthetic compounds in the future to enhance the safety and reduce the toxicity on normal cell lines, it is suggested to prepare halogenated derivatives that may have a positive effect on kinase enzymes.^{66,67} Moreover, to mitigate the toxicity on normal cells, the next steps will involve developing nanocarriers of the most active compounds specifically designed to target cancer cells instead of normal cells.^{68,69}

4. CONCLUSIONS

A new set of 2-aminobenzothiazole and 2-aminobenzothiazole–piperazine hybrid compounds were synthesized by aromatic nucleophilic substitution of monochloroacetyl chloride with chlorine. Alternatively, solvent-free or neat fusion can be used with various amines. The compounds were characterized and evaluated for PI3K γ inhibition and cytotoxic activity against MCF-7 and A549 cancer cell lines. Final compounds with 4-nitroaniline structures showed the highest activity against MCF-7 and A549 cancer cells, with IC₅₀ values ranging from 22.13 to 61.03 μ M. While OMS14 displayed a limited effect against PI3K γ , it showed significant inhibition (65%) against another cancer enzyme, PIK3CD/PIK3R1 (p110 δ /p85 α), suggesting a potential basis for its anticancer activity. NCI 60-cell line analysis of compounds OMS5 and OMS14 shows a broad-spectrum anticancer property, which suggests a potential lead for further preclinical analysis. Furthermore, we recognize the necessity to investigate specific strategies of targeted delivery. Our objective is to utilize these methods to achieve targeted treatment, increasing the selectivity toward cancer cells while limiting its effects on healthy cells.

As we continue, we will concentrate on improving and optimizing the most potent drugs, aiming to decrease the harmful effects on healthy cells while simultaneously enhancing the effectiveness against cancer. These efforts highlight the potential of these molecules as attractive candidates for future therapeutic approaches. The study we conducted provides vital insights into the design and evaluation of anticancer agents. We

expect that this will lead to greater progress in the preclinical development of these molecules.

■ ASSOCIATED CONTENT

Supporting Information

The Supporting Information is available free of charge at <https://pubs.acs.org/doi/10.1021/acsomega.3c09212>.

Smile file for the aminobenzothiazole synthetic compounds (OMS1–OMS16) (Table S1); one ADMET properties of synthetic compounds (OMS1–OMS16) (Table S2); toxicity prediction, model: TOPKAT rat oral LD50 (Table S3); NCI 60-cell line inhibition of OMS5 (Figure S1); NCI 60-cell line inhibition of OMS14 (Figure S2); IR spectrum of OMS1–OMS14 (Figures S3–S19); mass spectrum of compounds OMS1–OMS14 (Figures S20–S36); and ¹H-NMR spectrum and ¹³C-NMR spectrum of compounds OMS1–OMS14 (Figures S37–S70) (PDF)

■ AUTHOR INFORMATION

Corresponding Author

Mahmoud A. Al-Sha'er – Pharmaceutical Sciences Department, College of Pharmacy, Zarqa University, Zarqa 13132, Jordan; orcid.org/0000-0001-9962-1971; Email: a.mahmoud@zu.edu.jo

Authors

Omar M. Salih – Pharmaceutical Sciences Department, College of Pharmacy, Zarqa University, Zarqa 13132, Jordan

Haneen A. Basheer – Clinical Pharmacy Department, College of Pharmacy, Zarqa University, Zarqa 13132, Jordan

Complete contact information is available at:

<https://pubs.acs.org/10.1021/acsomega.3c09212>

Funding

The project was funded by Zarqa University's Research Department under the fund code M3–2020 as a master's project for Omar M. Salih.

Notes

The authors declare no competing financial interest.

■ ACKNOWLEDGMENTS

The authors thank the National Cancer Institute Developmental Therapeutics Program (NCI/DTP) <https://dtp.cancer.gov> for providing screening data for compounds presented in this manuscript, specifically, NSCs 848880 and 848881 for their support through the NCI 60-cell line assay. The authors are also thankful to Zarqa University's Deanship of Scientific Research for funding the endeavor and to Ahmed Mahdi, Dr. Laith Mahdi, Dr. Othman Makki, Dr. Omar Jamal, and Professor Mahmoud Ahmad Mousa Al-Elaimat for providing chemicals, instruments, IR, GC-MS, and NMR compound analysis. This document is part of the Zarqa University College of Pharmacy student Omar M. Salih's pharmaceutical sciences master's thesis.

■ REFERENCES

- (1) Novio, S.; Núñez-Iglesias, M. J.; Freire-Garabal, M. Isothiocyanates, Epigenetics, and Cancer Prevention. In *Epigenetics of Cancer Prevention*; Academic Press, 2019; pp 149–168.
- (2) Bray, F. F. J. S.; Ferlay, J.; Soerjomataram, I.; Siegel, R. L.; Torre, L. A.; Jemal, A. J. C. C. J. C. Erratum: Global cancer statistics 2018:

- GLOBOCAN estimates of incidence and mortality worldwide for 36 cancers in 185 countries. *Ca-Cancer J. Clin.* **2020**, *70* (4), 313.
- (3) Wilkinson, L.; Gathani, T. Understanding breast cancer as a global health concern. *Br. J. Radiol.* **2022**, *95* (1130), No. 20211033.
- (4) Shi, M.; Qiufeng, C.; Luming, Y.; Yubin, M.; Yanlin, M.; Gaoliang, O. Antiproliferation and apoptosis induced by curcumin in human ovarian cancer cells. *Cell Biol. Int.* **2006**, *30* (3), 221–226.
- (5) Peng, Y.; Wang, Y.; Zhou, C.; Mei, W.; Zeng, C. PI3K/Akt/mTOR Pathway and Its Role in Cancer Therapeutics: Are We Making Headway? *Front. Oncol.* **2022**, *12*, No. 819128.
- (6) Li, H.; Prever, L.; Hirsch, E.; Gulluni, F. Targeting PI3K/AKT/mTOR signaling pathway in breast cancer. *Cancers* **2021**, *13* (14), 3517.
- (7) Duan, Y.; Haybaeck, J.; Yang, Z. Therapeutic potential of PI3K/AKT/mTOR pathway in gastrointestinal stromal tumors: rationale and progress. *Cancers* **2020**, *12* (10), 2972.
- (8) Iksen; Pothongsrisit, S.; Pongrakhananon, V. Targeting the PI3K/AKT/mTOR signaling pathway in lung cancer: an update regarding potential drugs and natural products. *Molecules* **2021**, *26* (13), 4100.
- (9) Manzari, M. T.; Shamay, Y.; Kiguchi, H.; Rosen, N.; Scaltriti, M.; Heller, D. A. Targeted drug delivery strategies for precision medicines. *Nat. Rev. Mater.* **2021**, *6* (4), 351–370.
- (10) Zhong, L.; Li, Y.; Xiong, L.; Wang, W.; Wu, M.; Yuan, T.; Yang, S.; et al. Small molecules in targeted cancer therapy: Advances, challenges, and future perspectives. *Signal Transduction Targeted Ther.* **2021**, *6* (1), No. 201.
- (11) O'Donnell, J. S.; Massi, D.; Teng, M. W.; Mandala, M. PI3K-AKT-mTOR inhibition in cancer immunotherapy, redux. In *Seminars in Cancer Biology*; Academic Press, 2018, February; Vol. 48, pp 91–103.
- (12) Hanahan, D.; Weinberg, R. A. Hallmarks of cancer: the next generation. *Cell* **2011**, *144* (5), 646–674.
- (13) Rodon, J.; Dienstmann, R.; Serra, V.; Tabernero, J. Development of PI3K inhibitors: lessons learned from early clinical trials. *Nat. Rev. Clin. Oncol.* **2013**, *10* (3), 143–153.
- (14) Evans, C. A.; Liu, T.; Lescarbeau, A.; Nair, S. J.; Grenier, L.; Pradeilles, J. A.; Castro, A. C.; et al. Discovery of a selective phosphoinositide-3-kinase (PI3K)- γ inhibitor (IPI-549) as an immuno-oncology clinical candidate. *ACS Med. Chem. Lett.* **2016**, *7* (9), 862–867.
- (15) Patel, R. V.; Kumari, P.; Rajani, D. P.; Chikhaliya, K. H. Synthesis and studies of novel 2-(4-cyano-3-trifluoromethylphenyl amino)-4-(quinoline-4-yloxy)-6-(piperazinyl/piperidinyl)-s-triazines as potential antimicrobial, antimycobacterial and anticancer agents. *Eur. J. Med. Chem.* **2011**, *46* (9), 4354–4365.
- (16) Sharma, P. C.; Sinhmar, A.; Sharma, A.; Rajak, H.; Pathak, D. P. Medicinal significance of benzothiazole scaffold: an insight view. *J. Enzyme Inhib. Med. Chem.* **2013**, *28* (2), 240–266.
- (17) Zhilitskaya, L. V.; Shainyan, B. A.; Yarosh, N. O. Modern Approaches to the Synthesis and Transformations of Practically Valuable Benzothiazole Derivatives. *Molecules* **2021**, *26* (8), 2190.
- (18) Ray, P.; Clément, M.; Martini, C.; Abdellah, I.; Beauvier, P.; Rodriguez-Lopez, J. L.; Huc, V.; Remita, H.; Lampre, I. Stabilization of small mono- and bimetallic gold–silver nanoparticles using calix[8]-arene derivatives. *New J. Chem.* **2018**, *42* (17), 14128–14137.
- (19) Bele, D. S.; Singhvi, I. Synthesis and Analgesic Activity of Some Mannich Bases of 6-Substituted-2-Aminobenzothiazole. *Res. J. Pharm. Tech.* **2008**, *1* (1), 22–24.
- (20) Venkatesh, P.; Pandeya, S. N. (2009). Synthesis, characterization, and anti-inflammatory activity of some 2-amino benzothiazole derivatives.
- (21) Liu, Y.; Wang, Y.; Dong, G.; Zhang, Y.; Wu, S.; Miao, Z.; Sheng, C.; et al. Novel benzothiazole derivatives with a broad antifungal spectrum: Design, synthesis and structure–activity relationships. *MedChemComm* **2013**, *4* (12), 1551–1561.
- (22) Padalkar, V. S.; Gupta, V. D.; Phatangare, K. R.; Patil, V. S.; Umape, P. G.; Sekar, N. Synthesis of novel dipodal-benzimidazole, benzoxazole, and benzothiazole from cyanuric chloride: Structural, photophysical and antimicrobial studies. *J. Saudi Chem. Soc.* **2014**, *18* (3), 262–268.
- (23) Cai, J.; Sun, M.; Wu, X.; Chen, J.; Wang, P.; Zong, X.; Ji, M. Design and synthesis of novel 4-benzothiazole amino quinazolines Dasatinib derivatives as potential anti-tumor agents. *Eur. J. Med. Chem.* **2013**, *63*, 702–712.
- (24) Delmas, F.; Avellaneda, A.; Di Giorgio, C.; Robin, M.; De Clercq, E.; Timon-David, P.; Galy, J. P. Synthesis and antileishmanial activity of (1, 3-benzothiazol-2-yl) amino-9-(10H)-acridinone derivatives. *Eur. J. Med. Chem.* **2004**, *39* (8), 685–690.
- (25) Munirajasekar, D.; Himaja, M.; Sunil, M. Synthesis and anthelmintic activity of 2-amino-6-substituted benzothiazoles. *Int. Res. J. Pharm.* **2011**, *2* (2), 114–117.
- (26) Yadav, P. S.; Devprakash, D.; Senthilkumar, G. P. Benzothiazole: different methods of synthesis and diverse biological activities. *Int. J. Pharm. Sci. Drug Res.* **2011**, *3* (1), 1–7.
- (27) Siddiqui, N.; Rana, A.; Khan, S. A.; Bhat, M. A.; Haque, S. E. Synthesis of benzothiazole semicarbazones as novel anticonvulsants—The role of hydrophobic domain. *Bioorg. Med. Chem. Lett.* **2007**, *17* (15), 4178–4182.
- (28) Suresh, A. J.; Kumar, B.; Ramakrishnan, S. P. Design, synthesis, characterization, and biological evaluation of some novel benzothiazole derivatives as anti-tubercular agents targeting glutamine synthetase-I. *J. Pharm. Chem. Biol. Sci.* **2018**, *5* (4), 312–319.
- (29) Palkar, M.; Noolvi, M.; Sankangoud, R.; Maddi, V.; Gadad, A.; Nargund, L. V. G. Synthesis and Antibacterial Activity of a Novel Series of 2, 3-Diaryl-substituted-imidazo (2, 1-b)-benzothiazole Derivatives. *Arch. Pharm.* **2010**, *343* (6), 353–359.
- (30) Diao, P.-C.; Wei-Yuan, L.; Xie-Er, J.; Yan-Hong, L.; Wen-Wei, Y.; Pei-Liang, Z. Discovery of novel pyrimidine-based benzothiazole derivatives as potent cyclin-dependent kinase 2 inhibitors with anticancer activity. *Eur. J. Med. Chem.* **2019**, *179*, 196–207.
- (31) Kim, J.; Hong, S. H.; Jeon, S. H.; Park, M. H.; Shin, C.-G. The Novel Benzothiazole Derivative PB11 Induces Apoptosis via the PI3K/AKT Signaling Pathway in Human Cancer Cell Lines. *Int. J. Mol. Sci.* **2021**, *22* (5), 2718.
- (32) D'Angelo, N. D.; Kim, T.-S.; Andrews, K.; Booker, S. K.; Caenepeel, S.; Chen, K.; D'Amico, D.; Freeman, D.; Jiang, J.; Liu, L.; McCarter, J. D.; Miguel, T. S.; Mullady, E. L.; Schrag, M.; Subramanian, R.; Tang, J.; Wahl, R. C.; Wang, L.; Whittington, D. A.; Wu, T.; Xi, N.; Xu, Y.; Yakowec, P.; Yang, K.; Zalameda, L. P.; Zhang, N.; Hughes, P.; Norman, M. H. Discovery and optimization of a series of benzothiazole phosphoinositide 3-kinase (PI3K)/mammalian target of rapamycin (mTOR) dual inhibitors. *J. Med. Chem.* **2011**, *54* (6), 1789–1811.
- (33) Gabr, M. T.; El-Gohary, N. S.; El-Bendary, E. R.; El-Kerdawy, M. M. New series of benzothiazole and pyrimido [2, 1-b] benzothiazole derivatives: synthesis, antitumor activity, EGFR tyrosine kinase inhibitory activity and molecular modeling studies. *Med. Chem. Res.* **2015**, *24* (2), 860–878.
- (34) Song, X.; Xia, Y.; Wang, N.; Zhang, L.; Shi, X.; Xu, Y.; Ye, T.; Shi, Y.; Zhu, Y.; Luoting, Y. A novel benzothiazole derivative YLT322 induces apoptosis via the mitochondrial apoptosis pathway in vitro with anti-tumor activity in solid malignancies. *PLoS One* **2013**, *8* (5), No. e63900.
- (35) Boumendjel, A.; Nicolle, E.; Moraux, T.; Gerby, B.; Blanc, M.; Ronot, X.; Boutonnat, J. Piperazinobenzopyranones and phenalkylaminobenzopyranones: potent inhibitors of breast cancer resistance protein (ABCG2). *J. Med. Chem.* **2005**, *48* (23), 7275–7281.
- (36) Tuncbilek, M.; Bilget Guven, E.; Onder, T.; Cetin Atalay, R. Synthesis of novel 6-(4-substituted piperazine-1-yl)-9-(β -d-ribofuranosyl) purine derivatives, which lead to senescence-induced cell death in liver cancer cells. *J. Med. Chem.* **2012**, *55* (7), 3058–3065.
- (37) Al-Soud, Y. A.; Al-Sa'doni, H. H.; Saeed, B.; Jaber, I. H.; Beni-Khalid, M. O.; Al-Masoudi, N. A.; Loddo, R.; et al. Synthesis and in vitro antiproliferative activity of new benzothiazole derivatives. *ARKIVOC* **2008**, *2008*, 225–238.
- (38) Gurdal, E. E.; Durmaz, I.; Cetin-Atalay, R.; Yarim, M. Cytotoxic activities of some benzothiazole-piperazine derivatives. *J. Enzyme Inhib. Med. Chem.* **2015**, *30* (4), 649–654.
- (39) Alelaimat, M. A.; Al-Sha'er, M. A.; Basheer, H. A. Novel Sulfonamide-Triazine Hybrid Derivatives: Docking, Synthesis, and

- Biological Evaluation as Anticancer Agents. *ACS omega* **2023**, *8* (15), 14247–14263.
- (40) Rathinaswamy, M. K.; Gaieb, Z.; Fleming, K. D.; Borsari, C.; Harris, N. J.; Moeller, B. E.; Burke, J. E.; et al. Disease-related mutations in PI3K γ disrupt regulatory C-terminal dynamics and reveal a path to selective inhibitors. *eLife* **2021**, *10*, No. e64691.
- (41) Ramírez, D.; Caballero, J. Is it reliable to take the molecular docking top-scoring position as the best solution without considering available structural data? *Molecules* **2018**, *23* (5), 1038.
- (42) Li, D.; Rui, Y. X.; Guo, S. D.; Luan, F.; Liu, R.; Zeng, N. Ferulic acid: A review of its pharmacology, pharmacokinetics and derivatives. *Life Sci.* **2021**, *284*, No. 119921.
- (43) Cheng, A.; Dixon, S. L. In silico models for the prediction of dose-dependent human hepatotoxicity. *J. Comput.-Aided Mol. Des.* **2003**, *17*, 811–823.
- (44) Bhargava, P. N.; Ram, P. The synthesis of local anesthetics. *Bull. Chem. Soc. Jpn.* **1965**, *38* (3), 339–341.
- (45) Altintop, M. D.; Kaplancikli, Z. A.; Ozdemir, A.; Turan-Zitouni, G.; Temel, H. E.; Akalin, G. Synthesis and anticholinesterase activity and cytotoxicity of novel amide derivatives. *Archiv der Pharmazie* **2012**, *345* (2), 112–116.
- (46) Baraldi, P. G.; Preti, D.; Tabrizi, M. A.; Fruttarolo, F.; Saponaro, G.; Baraldi, S.; Borea, P. A.; et al. N6-[(Hetero) aryl/(cyclo) alkyl-carbamoyl-methoxy-phenyl]-(2-chloro)-5'-N-ethylcarboxamido-adenosines: The first example of adenosine-related structures with potent agonist activity at the human A2B adenosine receptor. *Bioorg. Med. Chem.* **2007**, *15* (7), 2514–2527.
- (47) Zhaowen, L.; Li, Z.; Chunfen, X.; Yong, Y.; Fanbo, Z.; Kaixun, H. Anticancer activities of some arylcarbamoylalkyltriphenylphosphonium chlorides. *Medicinal Chemistry Research* **2007**, *16*, 380–391.
- (48) Al-Sha'er, M. A.; Taha, M. O. Application of docking-based comparative intermolecular contacts analysis to validate Hsp90 α docking studies and subsequent in silico screening for inhibitors. *J. Mol. Model.* **2012**, *18*, 4843–4863.
- (49) Tahir, S.; Mahmood, T.; Dastgir, F.; Haq, I. U.; Waseem, A.; Rashid, U. Design, synthesis, and anti-bacterial studies of piperazine derivatives against drug-resistant bacteria. *Eur. J. Med. Chem.* **2019**, *166*, 224–231.
- (50) Quinn, T. J.; Galoforo, S.; Wilson, T. G.; Ahmed, S.; Wilson, G. D. Dual EGFR and PI3k/mTOR Targeting of Head and Neck Cancer in Combination With Radiation Therapy. *Int. J. Radiat. Oncol., Biol., Phys.* **2017**, *99* (2), E614–E615.
- (51) Nagahama, K.; Kawano, D.; Oyama, N.; Takemoto, A.; Kumano, T.; Kawakami, J. Self-assembling polymer micelle/clay nanodisk/doxorubicin hybrid injectable gels for safe and efficient focal treatment of cancer. *Biomacromolecules* **2015**, *16* (3), 880–889.
- (52) Su, Q.; Xu, B.; Tian, Z.; Gong, Z. Design and development of novel 1, 2, 3-triazole chalcone derivatives as potential anti-osteosarcoma agents via inhibition of PI3K/Akt/mTOR signaling pathway. *Acta Pharm.* **2022**, *72* (3), 389–402.
- (53) Wu, T. T.; Guo, Q. Q.; Chen, Z. L.; Wang, L. L.; Du, Y.; Chen, R.; Zhang, J. Q.; et al. Design, synthesis, and bioevaluation of novel substituted triazines as potential dual PI3K/mTOR inhibitors. *Eur. J. Med. Chem.* **2020**, *204*, No. 112637.
- (54) Kashkin, K. N.; Musatkina, E. A.; Komelkov, A. V.; Favorskaya, I. A.; Trushkin, E. V.; Shleptsova, V. A.; Sverdlov, E. D. Expression profiling and putative mechanisms of resistance to doxorubicin of human lung cancer cells. In *Doklady. Biochemistry and Biophysics*; Springer Nature BV, 2010, February; Vol. 430, p 20.
- (55) Kopecka, J.; Rankin, G. M.; Salaroglio, I. C.; Poulsen, S. A.; Riganti, C. P-glycoprotein-mediated chemoresistance is reversed by carbonic anhydrase XII inhibitors. *Oncotarget* **2016**, *7* (52), 85861.
- (56) Liu, C.; Xing, W.; Yu, H.; Zhang, W.; Si, T. ABCB1 and ABCG2 restrict the efficacy of gedatolisib (PF-05212384), a PI3K inhibitor in colorectal cancer cells. *Cancer Cell Int.* **2021**, *21* (1), 108.
- (57) Khamis, M. A.; Gomaa, W.; Ahmed, W. F. Machine learning in computational docking. *Artificial intelligence in medicine* **2015**, *63* (3), 135–152.
- (58) Morris, G. M.; Lim-Wilby, M. Molecular docking. *Methods Mol. Biol.* **2008**, *443*, 365–382.
- (59) Diller, D. J.; Merz, K. M., Jr. High throughput docking for library design and library prioritization. *Proteins: Struct., Funct., Bioinf.* **2001**, *43* (2), 113–124.
- (60) Jain, A. N. Effects of protein conformation in docking: improved pose prediction through protein pocket adaptation. *J. Comput.-Aided Mol. Des.* **2009**, *23*, 355–374.
- (61) Cheng, T.; Li, X.; Li, Y.; Liu, Z.; Wang, R. Comparative assessment of scoring functions on a diverse test set. *J. Chem. Inf. Model.* **2009**, *49* (4), 1079–1093.
- (62) Gohlke, H.; Klebe, G. Approaches to the description and prediction of the binding affinity of small-molecule ligands to macromolecular receptors. *Angew. Chem., Int. Ed.* **2002**, *41* (15), 2644–2676.
- (63) Huang, G.; Cierpicki, T.; Grembecka, J. 2-Aminobenzothiazoles in anticancer drug design and discovery. *Bioorg. Chem.* **2023**, *135*, No. 106477.
- (64) DTP Website: <http://dtp.nci.nih.gov/>; Compound Submissions: <http://dtp.nci.nih.gov/compsub/index.html>.
- (65) Thermofisher. Z'-LYTE, Kinase Assay. <https://www.thermofisher.com/> 2021.
- (66) Al-Sha'er, M. A.; Almazari, I. S.; Taha, M. O. Discovery of novel potent nuclear factor kappa-B inhibitors (IKK- β) via extensive ligand-based modeling and virtual screening. *J. Mol. Recognit.* **2017**, *30* (6), No. e2604.
- (67) Al-Sha'er, M. A.; Taha, M.; Alelaimat, M. A. Development of phosphoinositide 3-kinase delta (PI3K δ) inhibitors as potential anticancer agents through the generation of ligand-based pharmacophores and biological screening. *Med. Chem. Res.* **2023**, *32*, 1109–1121.
- (68) Vieira, D. B.; Gamarra, L. F. Advances in the use of nanocarriers for cancer diagnosis and treatment. *Einstein (Sao Paulo)* **2016**, *14* (1), 99–103.
- (69) Yu, B.; Tai, H. C.; Xue, W.; Lee, L. J.; Lee, R. J. Receptor-targeted nanocarriers for therapeutic delivery to cancer. *Mol. Membr. Biol.* **2010**, *27* (7), 286–298.